MASS-SELECTIVE VIBRATIONAL SPECTROSCOPY OF VANADIUM OXIDE CLUSTER IONS

Knut R. Asmis[1]* and Joachim Sauer[2]
[1]*Fritz-Haber-Institut der Max-Planck-Gesellschaft, Faradayweg 4-6, D-14195 Berlin, Germany*
[2]*Institut für Chemie, Humboldt-Universität Berlin, Unter den Linden 6, 10099 Berlin, Germany*

Received 10 June 2006; received (revised) 12 October 2006; accepted 14 October 2006

Published online 23 May 2007 in Wiley InterScience (www.interscience.wiley.com) DOI 10.1002/mas.20136

A corner stone in the study of the size-dependent properties of cluster ions in the gas phase is their structural characterization. Over the last 10 years, significant progress has been made in this research field because of important advances in the gas phase vibrational spectroscopy of mass-selected ions. Using a combination of modern experimental and quantum chemical approaches, it is now in most cases possible to uniquely identify the geometric structure of cluster ions, based on the comparison of the experimental and simulated infrared spectra. In this article, we highlight the progress made in this research area by reviewing recent infrared photodissociation experiments on small and medium sized vanadium oxide ions. © 2007 Wiley Periodicals, Inc., Mass Spec Rev 26:542–562, 2007

Keywords: *vanadium oxide clusters; infrared photodissociation spectroscopy; messenger atom; density functional theory (DFT); electron localization; cluster size effects*

I. INTRODUCTION

Over the last 10 years, substantial progress has been made in the study of the size-dependent properties of mass-selected cluster ions in the gas phase. These studies are motivated not only by the interest in this peculiar state of matter, but also, for example, by the need to aid in the design of functional building blocks for nanostructured materials (Siegel, Hu, & Roco, 1999), and by the desire to gain a better understanding of the elementary steps in heterogeneous catalysis (Böhme & Schwarz, 2005). Cluster studies are also crucial in getting benchmark data for the assessment of quantum mechanical methods which can then be applied to systems for which no reliable structure data are available from experiment.

A corner stone in these studies is the structural characterization of cluster ions based on mass-selective gas phase vibrational spectroscopy. Using modern experimental and quantum chemical approaches, it is now in most cases possible to uniquely identify the geometric structure of mass-selected cluster ions, based on the comparison of the experimental and simulated infrared spectra. In this review, we highlight the progress made in this research area by describing, how recent infrared photodissociation (IR-PD) experiments using a tunable IR free electron laser (FEL) allowed for a systematic study of the gas phase vibrational spectroscopy of small and medium sized (~30 atoms) vanadium oxide ions.

This review starts with a brief motivation for performing experiments on vanadium oxide clusters, followed by an overview of previous gas phase spectroscopic studies aimed at identifying the geometric structure of these species. Section 2 presents an introduction to IR-PD spectroscopy using FEL radiation, including a brief description of the experimental apparatus, the working principle of FELs, and the mechanism of infrared multiple photon photodissociation (IR-MPD). Then the quantum chemical methods are described in Section 3, which are used to calculate the cluster structure, energetics, and vibrational frequencies. In Section 4, an overview of the measured IR-PD and assigned cluster structures is given, followed by a discussion of several important aspects related to the IR-PD spectroscopy of vanadium oxide ions. The review ends with an outlook on current and future developments in the field (Section 5).

A. Motivation

While vanadium oxides are important as cathode materials in lithium batteries (Whittingham, 2004), in bolometric detectors (de Almeida et al., 2004), and as ferromagnetic nanotubes (Krusin-Elbaum et al., 2004), it is their use as supported catalysts (Weckhuysen & Keller, 2003) that has motivated many recent cluster studies. Prominent examples are the use of vanadium oxide based catalysts in the synthesis of important bulk chemicals like SO_3, propene, phthalic, and maleic anhydride, and in the reduction of environmental pollution, for example, the selective reduction of nitrogen oxides NO_x in exhaust gas from power plants. Supported vanadium oxides show a large structural variability ranging from isolated sites over polymeric species to microcrystallites of bulk V_2O_5. The activity and selectivity of supported metal oxide catalysts are significantly affected by the properties of the support. Studying their structures and reactivities in the gas phase yields information about vanadium oxide species separated from the support. By comparison with surface science studies and/or theoretical studies of supported vanadium oxide species, information about the vanadium oxide support interaction is obtained.

Contract grant sponsor: Collaborative Research Center 546 of the Deutsche Forschungsgemeinschaft.
**Correspondence to:* Knut R. Asmis, Fritz-Haber-Institut der Max-Planck-Gesellschaft, Faradayweg 4-6, D-14195 Berlin, Germany.
E-mail: asmis@fhi-berlin.mpg.de

A promising experimental approach to shed light on the relationship between geometric structure and observed reactivity patterns involves performing reactivity measurements on size-selected clusters and cluster ions in the gas phase under well controlled conditions (Rudnyi, Kaibicheva, & Sidorov, 1993; Bell, Zemski, & Castleman, 1998, 1999a,b,c; Bell et al., 1998b; Dinca et al., 1999; Harvey et al., 1999; Bell et al., 2001; Koyanagi et al., 2001; Zemski, Justes, & Castleman, 2001, 2002; Bell & Castleman, 2002; Fielicke & Rademann, 2002; Engeser et al., 2003; Justes et al., 2003a,b; Justes, Moore, & Castleman, 2004; Schröder et al., 2004; Engeser, Schröder, & Schwarz, 2005; Feyel, Schröder, & Schwarz, 2006; Moore et al., 2006; Schröder et al., 2006). The lack of experimentally determined structures together with the lack of thermochemical data, however, has hindered the identification of structure-reactivity relationships. The reverse procedure, predicting structures from observed reactivity patterns of vanadium oxide cations (Bell et al., 1998b) has not met with success as later structure determinations showed (Asmis et al., 2004). While the size and composition of the reactants and products can be characterized using mass spectrometry, their geometric structure can, in principle, be predicted by quantum chemical approaches (Vyboishchikov & Sauer, 2000, 2001; Calatayud, Andrés, & Beltrán, 2001; Calatayud et al., 2001b; Pykavy & van Wüllen, 2003; Pykavy, van Wüllen, & Sauer, 2004; Sauer & Döbler, 2004). In practice, the reliable structure prediction is complicated by the lack of an algorithm for finding the absolute energy minimum on a complex potential energy surface in combination with many low-energy isomers and low-lying electronic states. Several previous computational studies on smaller vanadium oxide cations, for example, disagreed on the lowest electronic state and the global minimum structure, even though they applied very similar computational techniques (Koyanagi et al., 2001; Calatayud, Andrés, & Beltrán, 2001; Calatayud et al., 2001b; Justes et al., 2003b). For neutral vanadium oxide clusters, Matsuda and Bernstein (2005) predict closed shell singlet ground states for systems with an even number of electrons, which is in conflict with previous calculations (Pykavy & van Wüllen, 2003; Pykavy, van Wüllen, & Sauer, 2004). Therefore, a reliable identification of the cluster structure generally requires the confirmation by experimental data, for example, from vibrational spectroscopy (Asmis et al., 2004, 2005).

B. Vibrational Spectroscopy: Previous Experiments

Prior to the IR-PD experiments discussed in this review, the vibrational spectroscopy of isolated polyatomic vanadium oxide species had been limited to the study of a few neutral clusters (see Table 1) using IR matrix absorption (IR-MA) and anion photoelectron (APE) spectroscopy. Initial studies focused on the diatomic VO (Keenan & Schroeder, 1952; Lagerqvist & Selin, 1957), motivated by its near infrared emission in the spectra of M-type stars. VO has a $^4\Sigma^-$ ground state (Kasai, 1968; Knight et al., 1996) with fundamental constants $\omega_0 = 1001.8$ cm^{-1} and $r_0 = 1.592$ Å in the gas phase (Merer, 1989). Formal removal of an electron from the vanadium 4s orbital leads to VO^+ in its $^3\Sigma^-$ ground state and a strengthening of the V=O bond ($\omega_0 = 1060 \pm 40$ cm^{-1}, $r_0 = 1.56$ Å) (Dyke et al., 1985; Harrington & Weisshaar, 1992). Stimulated by mass spectrometric studies (Berkowitz, Chupka, & Inghram, 1957; Farber, Srivastava, & Uy, 1972), which had found V_4O_{10} and V_4O_8 as prominent vapor species above heated vanadium pentoxide, Beattie, Ogden, and Price (1978) observed two strong absorptions at 1030 and 828 cm^{-1} in the IR-MA spectrum of V_2O_5 vapor codeposited with N_2 and assigned them, in analogy to P_4O_{10}, to the terminal (V=O) and bridge (V–O–V) modes, respectively, of neutral V_4O_{10}. The vibrational spectroscopy of other isolated polyatomic vanadium oxide species, neutral or ionic, remained unexplored, until the IR-MA studies by Andrews and co-workers on VO_2, VO_4, and V_2O_{2-4} (Chertihin, Bare, & Andrews, 1997).

Wang and co-workers applied APE spectroscopy to vanadium oxide clusters (Wu & Wang, 1998; Zhai & Wang, 2002). APE spectroscopy is a powerful technique to measure electron detachment energies of negative ions, which can yield vibrational information on the neutral cluster, mainly for smaller systems. For example, the APE spectra of VO_2^- place the ν_1 frequency of neutral VO_2 at 970 cm^{-1} in the gas phase (Wu & Wang, 1998), in reasonable agreement with the IR-MA data (946 cm^{-1}), which had found a bent O–V–O structure (Chertihin, Bare, & Andrews, 1997). Structural assignments for the larger clusters were more difficult. The APE spectra of divanadium oxide anions support a common V–O–V–O ring motif for V_2O_3 to V_2O_7, with additional oxygen atoms adding to the V atoms. However, vibrational frequencies are only resolved for V_2O_4 (1090 cm^{-1}) and V_2O_6 (800 cm^{-1}), not sufficient for a definitive structural assignment. Vibrationally resolved APE data has also been reported for V_3O^-, supporting a planar structure containing a V_3 ring doubly bridged to the oxygen atom (Green et al., 2001).

II. EXPERIMENTAL SECTION

A. Infrared Photodissociation Spectroscopy

Vibrational spectroscopy paired with quantum chemistry currently offers one of the most direct and generally applicable experimental approaches to structural investigation of neutral and charged cluster in the gas phase (Bieske & Dopfer, 2000; Duncan, 2000). Direct absorption measurements based on discharge modulation methods (Rosenbaum et al., 1986) can yield high-resolution spectra of small and light molecular ions. Problems associated with high-discharge temperatures can currently be overcome by using pulsed-slit supersonic expansions (Davis et al., 2001). However, these types of experiments become increasingly difficult for larger and heavier molecular ions, particularly ion clusters, owing to spectral congestion, lower gas phase number densities, and presence of other absorbing species. Therefore, alternative techniques have been developed in which the absorption of photons can be measured indirectly (action spectroscopy), for example, by way of (resonance enhanced) IR-MPD:

$$AB^+ \xrightarrow{n \cdot h\nu} A^+ + B \qquad (1)$$

Photodissociation techniques have the advantage that fragment ions can be detected background-free and with nearly 100%

TABLE 1. Overview of Experimental Studies on the Vibrational Spectroscopy of Isolated, Polyatomic Vanadium Oxide Clusters

system / charge state	anion	neutral	cation
VO_2		IR-MA[d], APE[e]	IR-VPD [h,i]
VO_3			IR-VPD [h,i]
VO_4		IR-MA[d]	
V_2O_2		IR-MA[d]	IR-VPD [i]
V_2O_3		IR-MA[d]	IR-VPD [i]
V_2O_4		IR-MA[d], APE[f]	IR-VPD [i]
V_2O_5			IR-VPD [i]
V_2O_6	IR-MPD[a]	APE[f]	IR-VPD [i]
V_2O_7	IR-MPD [a]		
V_3O	APE [b]	APE [b]	
V_3O_6			IR-VPD [j]
V_3O_7			IR-VPD [k]
V_3O_8	IR-MPD [a]		IR-MPD [l], IR-VPD [k]
V_4O_{10}	IR-MPD [a,c]	IR-MA [g]	IR-MPD [m]
V_4O_{11}	IR-MPD [a]		
V_4O_{12}			IR-MPD [n]
V_5O_{13}	IR-MPD [a]		
V_6O_{13}			IR-MPD [l]
V_6O_{15}	IR-MPD [a,c]		IR-MPD [l]
V_7O_{18}	IR-MPD [a]		
V_8O_{20}	IR-MPD [a,c]		

Experiments include IR-MA, APE, and neutral photoelectron (NPS), IR-VPD, and IR-MPD spectroscopy.

[a](Santambrogio et al., 2006).
[b](Green et al., 2001).
[c](Asmis et al., 2005).
[d](Chertihin, Bare, & Andrews, 1997).
[e](Wu & Wang, 1998).
[f](Zhai & Wang, 2002).
[g](Beattie, Ogden, & Price, 1978).
[h](Brümmer et al., 2003).
[i](Asmis et al., 2004).
[j]unpublished results.
[k](Gause, 2004).
[l](Santambrogio, 2001).
[m](Asmis et al., 2002).
[n](Kaposta, 2005).

detection efficiency. A high selectivity can be achieved through mass selection of parent and fragment ions using appropriate mass filters.

Infrared multiple photon photodissociation experiments generally require intense and tunable radiation sources which, until the middle 1990s, were commercially available only in the wavelength region up to ~4 μm (>2500 cm^{-1}) as well as narrow parts of the spectrum around 6 and 10 μm, accessible using CO and CO_2 laser radiation. This former wavelength range corresponds to O–H stretches, as well as a variety of overtones and combination bands. The characteristic vibrational signature of transition metal oxide bonds, however, is found at longer wavelengths, roughly in the 500–1600 cm^{-1} range. The application of FELs to molecular spectroscopy in 1996 has bridged this gap (Putter, von Helden, & Meijer, 1996; von Helden et al., 1997). The FEL used in these experiments generated intense (typically 20 mJ per 5 μs macro pulse) and continuously tunable IR radiation from 5 to 250 μm (2000–40 cm^{-1}) (Knippels et al., 1995; Oepts, van der Meer, & van Amersfoort, 1995). This opened the door to study the vibrational spectroscopy of molecular and cluster ions in the fingerprint region of the electromagnetic spectrum (von Helden, van Heijnsbergen, & Meijer, 2003).

B. Guided Ion Beam Tandem Mass Spectrometer

The experiments described here were performed on a guided ion beam tandem mass spectrometer (Asmis et al., 2002) that was temporarily installed at the FEL facility FEL for infrared experiments (FELIX, FOM Institute for Plasma Physics, Nieuwegein, The Netherlands) (Knippels et al., 1995; Oepts, van der Meer, & van Amersfoort, 1995). A schematic of the experimental setup is shown in Figure 1.

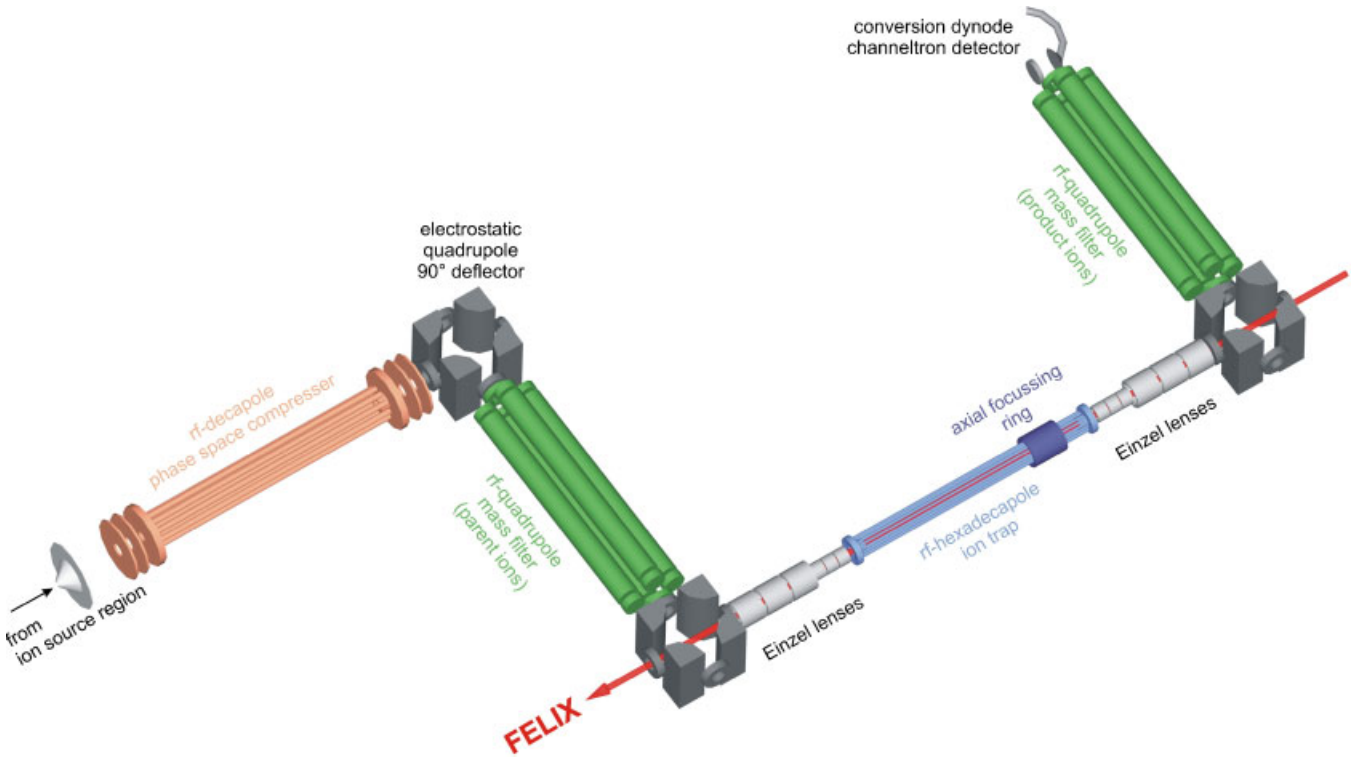

FIGURE 1. Schematic of the guided-ion-beam-tandem-mass-spectrometer used in the present studies.(Asmis et al., 2002) The instrument is housed in a 5-stage differentially pumped vacuum chamber. The FEL radiation is applied collinearly to the axis of the ion trap. [Color figure can be viewed in the online issue, which is available at www.interscience.wiley.com.]

Gas phase vanadium oxide ions are produced by laser vaporization (Asmis et al., 2002) in a Smalley-type (Dietz et al., 1981) source. The second harmonic of a Q-switched Nd:YAG laser is focused on a metal target. The target is rotated and translated to hit a fresh spot with every laser shot. The nanosecond laser pulse with typical pulse energies of a few millijoule impinges on the metallic target and the metal vapor produced by the early portion of the laser pulse forms a dense cloud near the metal surface. This cloud is quickly ionized and the resulting plasma is entrained in a buffer gas pulse and allowed to thermalize through collisions with the source walls in the expansion channel. Cluster formation occurs here through three-body-collisions. Adding small amounts of a reactive gas to the buffer gas allows tailoring the cluster composition. For example, the average oxygen content of metal oxide clusters can be tuned by the amount of oxygen added to the He seed gas. The gas pulse then expands into the vacuum cooling mainly the rotational and translational degrees of freedom. The vibrational temperature of the ions is determined mainly by the temperature of the source chamber.

The ion beam containing a distribution of cluster ions of different size exits the source region is collimated in space and compressed in phase space in a gas-filled radio frequency (RF) ion guide and directed into the first quadrupole mass filter. Mass-selected ions are then guided into a temperature-adjustable RF ion trap. The trap consists of a 22 cm long linear RF ion guide and two electrostatic ion lenses contained in a cylindrical housing, which is connected to the cold head of a closed-cycle He cryostat. The cylinder is continuously filled with He. The use of a buffer gas has several advantages. (i) The trap can be operated in a continuous ion-fill-mode. (ii) Trapped ions are collisionally cooled close to the ambient temperature (approximately within a few milliseconds). (iii) At low trap temperatures ion-messenger atom complexes can be formed. (iv) Adding a reactive gas to the buffer gas allows to study ion-molecule reactions. (v) Experiments can be performed at a defined, variable ion trap temperature, currently between 14 and 350 K.

Infrared photodissociation spectra are obtained by photoexcitation of the trapped ions with the pulsed FEL radiation and subsequent monitoring of the fragment ion signal. A new measurement cycle is triggered by the previous FEL macropulse. First, the ion trap is filled with mass-selected ions. The trap is then closed and the ions are allowed to thermalize. Directly after FELIX fires, all ions are extracted and the mass-selected ion yield is monitored. This cycle is repeated multiple times, the signal is summed and then the FEL is set to the next wavelength. The accuracy of the determined vibrational frequencies is generally within 1% of the central wavelength. The accuracy of the relative intensities is less well defined, mainly because of the non-monotonic variation of the FELIX beam intensity, bandwidth, and waist size with wavelength (von Helden et al., 1997; Oomens et al., 2003). We try to minimize these variations and do not correct for them in our spectra.

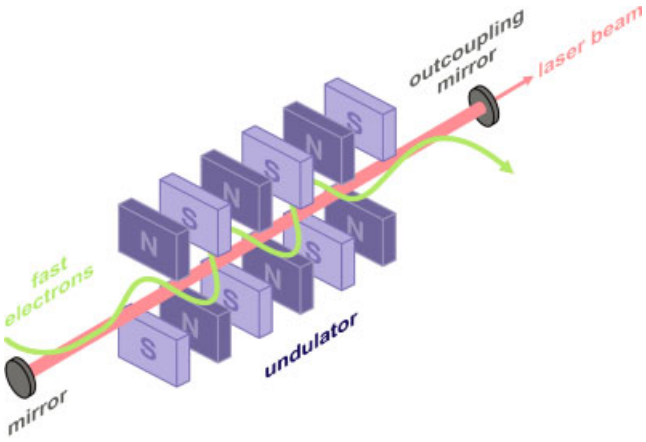

FIGURE 2. Schematic of an undulator used in FELs. [Color figure can be viewed in the online issue, which is available at www.interscience.wiley.com.]

C. The Free Electron Laser for Infrared Experiments (FELIX)

An FEL is a device which amplifies short-wavelength radiation by stimulated emission using a beam of relativistic electrons. The central part of an FEL is the undulator (Fig. 2), a periodically alternating static magnetic field. The peak emission wavelength depends on the undulator period L, the strength of the magnetic field expressed by a dimensionless parameter K, and the electron energy:

$$\lambda \propto \frac{L}{2\gamma^2}(1 + K^2). \tag{2}$$

$\gamma = mc^2/m_0c^2$ is the relativistic factor and corresponds to the kinetic energy of the electrons along the axis of the FEL in units of the electron rest energy m_0c^2. In the moving electron frame, the electrons see not only an oscillating magnetic field, but also an oscillating electric field in the perpendicular direction—in short, they see an electromagnetic wave with wavelength L/γ. Upon interaction with this wave the electrons emit (first-harmonic) light of the same wavelength. The corresponding wavelength in the laboratory frame is subject to the Doppler effect. Thus, for MeV electrons the macroscopic undulator period ($L \approx 1$ cm) is shortened by the Lorentz contraction ($1/\gamma$) and the Doppler shift ($1/2\gamma$) into the micrometer wavelength region.

The amount of power radiated spontaneously by a very energetic beam of electrons is not large. Indeed, if the electrons were spaced uniformly along the beam, there would be no power emitted at all because of negative interference. Only the fluctuations in particle current lead to a net radiation, which scales linearly with n, the number of electrons. The spectrum of the spontaneous radiation is determined by the finite undulator length $l = N{\cdot}L$, resulting in a finite transit time and a fractional width of the spontaneous or noise radiation of $1/N$.

The ponderomotive force acting between the axial electron velocity and the magnetic component of the electromagnetic wave is the origin of the stimulated emission of (highly coherent) photons. It couples the electron motion to the electromagnetic field and is phase dependent. Electrons that are in phase with the electromagnetic wave are retarded, whereas the ones with opposite phase gain energy. Through this exchange of energy a longitudinal density modulation on the scale of the wavelength is created, the so-called micro bunching. More and more electrons begin to radiate in phase, which results in an increasingly coherent superposition of the radiation emitted from the micro-bunched electrons. The more intense the electromagnetic field gets, the more pronounced the longitudinal density modulation of the electron bunch and vice versa (gain mechanism). With complete micro bunching, all electrons radiate almost in phase and this leads to a radiation power, which is proportional to N^2 and thus an amplification of many orders of magnitude with respect to the spontaneous emission of the undulator.

The temporal structure of the optical output pulse is determined by the incoming electron beam. The linear RF accelerators of FELIX typically generate 7 μs long pulse trains of 1 ps long electron bunches at a repetition rate of up to 10 Hz. The micropulse repetition rate is either 25 MHz or 1 GHz, the latter corresponding to 40 optical pulses circulating in the 6 m long cavity. The micropulse duration of the optical pulses can be varied from 300 fs to several ps and their bandwidth is near-transform limited, ranging from less than 0.5% to several percent full width at half maximum of the central wavelength.

The output wavelength of FELIX depends on the electron beam energy and the magnetic field strength. Generally, the wavelength is scanned by mechanically adjusting the distance of the undulator magnetic poles for fixed beam energy. A factor of three in wavelength can be covered using a single electron beam setting. Typically, macropulse energies at narrow bandwidth and 1 GHz micropulse repetition rate are 30–50 mJ. The IR radiation is guided via an evacuated transport system to a user station (roughly 30 m away).

D. IR-MPD Mechanism

The mechanism of (collisionless) IR-MPD for polyatomic molecules can be conceptually divided into three (overlapping) regions (Black et al., 1977):

(i) The polyatomic molecule is excited resonantly over discrete states into the quasi-continuum region.
(ii) The molecule continues to absorb photons resonantly, but this energy is quickly randomized among all vibrational degrees of freedom.
(iii) Once the internal energy reaches the dissociation limit, the molecule dissociates according to the statistical model of unimolecular reactions.

Region (i) is characterized by the coherent interaction of the radiation field with the discrete energy levels within a vibrational ladder. This resonantly enhanced multiphoton process is governed by selection rules for photoabsorption. The overall cross-section for excitation into the quasi-continuum depends on the laser frequency, the initial vibrational, and rotational temperature of the molecule and the laser peak intensity (in contrast to laser fluence). In the discrete region, small

anharmonic shifts of successive vibrational transitions within a single mode (''anharmonic bottleneck'') can be compensated for by changes in rotational quantum number, anharmonic splitting of excited degenerate vibrational states, and other effects. In the absence of such effects and in particular in small polyatomic molecules, for example, triatomic systems, two- and three-photon vibrational transitions, and thus higher peak intensities, may be necessary to reach the quasi-continuum. Under collisionless conditions, de-excitation of the vibrational levels can be neglected, because the time scale on which the multiphoton photodissociation process proceeds is much shorter than the typical lifetimes derived from spontaneous emission rates in the IR ($\sim 10^3$–10^4 s^{-1}).

With increasing internal energy E_i the density of rovibrational states $\sigma(E_i)$ increases very rapidly, roughly with E_i^N, where N is the number of vibrational degrees of freedom. Therefore, only a few photons are needed to reach the quasi-continuum region and for larger molecular systems the IR-MPD spectrum often resembles the linear absorption spectrum (Oomens, Meijer, & von Helden, 2001; Oomens et al., 2003, 2006). For smaller systems with fewer internal degrees of freedom, the relative intensities may be different. However, if the laser fluence is kept at a moderate level, signal is only detected, if the laser wavelength is resonant with a fundamental transition, that is,

$$AB^+(v=0) \xrightarrow{h\nu} AB^+(v=1) \xrightarrow{n' \cdot h\nu} A^+ + B \qquad (3)$$

At high laser fluence the probability of directly exciting overtones is enhanced, complicating the interpretation of the IR-MPD spectrum (Nee et al., 2004).

The energy deposition in the quasi-continuum region is mainly through stepwise incoherent one-photon transitions. The absorption properties of the quasi-continuum remain related to those of the discrete region. The absorption bands are generally red-shifted, because of mechanical cross-anharmonicities, and lifetime broadened. The latter is a direct consequence of the efficient intermode coupling in the quasi-continuum especially at higher energies, which results in rapid IVR. Typical timescales for intramolecular relaxation of highly excited polyatomic molecules are 10^{-11}–10^{-12} s, much faster than average dissociation lifetimes of several ns (Rynbrandt & Rabinovitch, 1971). Thus, photoabsorption in this region is always accompanied by randomization of the absorbed energy over the internal degrees of freedom and effective de-excitation of the absorbing transition, making it available for the absorption of another photon. Therefore, the cross-section for absorption in the quasi-continuum region is, in contrast to the discrete region, dependent on the energy fluence (time-integrated intensity) and not the peak intensity and is rate-limiting for the entire photodissociation process.

Once the internal energy of the molecule rises over the dissociation limit, the (true) continuum of levels is reached and a dissociative channel opens up. The originally bound states become metastable now and can be described in terms of decaying resonances because of coupling to the continuum states. The resonant excitation to higher levels is then always in competition with dissociation. As the dissociation rate is expected to increase rapidly with increasing internal energy, the up-excitation is quickly balanced by dissociation depleting the population. The distribution is thus different from a thermal distribution. The laser-excited population is narrower and asymmetric, because the high-energy tail is heavily depleted by dissociation (Grant et al., 1978). A simple phenomenological model (Grant et al., 1978; Sudbo et al., 1986) based on rate equations can be set up to describe the time-dependent excitation of the excited molecules to and beyond the dissociation limit.

E. Vibrational Predissociation: The Messenger Atom Technique

A useful method to avoid multiple photon excitation and measure IR photodissociation spectra in the linear regime is the messenger atom technique (Okumura, Yeh, & Lee, 1985):

$$AB^+ \cdot Rg \xrightarrow{h\nu} (AB^+ \cdot Rg)^* \rightarrow AB^+ + Rg \qquad (4)$$

By forming ion-rare gas atom (Rg) complexes the dissociation threshold of the system is lowered. Generally, one chooses the rare gas atom such that its binding energy to the cluster ion is below the photon energy and the infrared vibrational predissociation (IR-VPD) spectra, therefore, directly reflect the corresponding linear absorption spectra. This technique has also been used to great effect in anion spectroscopy experiments (Robertson & Johnson, 2003). For the present experiments messenger atom complexes with He and Ar were prepared by three-body collisions in the cold ion trap (Brümmer et al., 2003). The IR-MPD approach remains attractive for systems, in which the perturbation of the messenger atom cannot be neglected or for systems where rare gas attachment is difficult.

III. QUANTUM CHEMICAL METHODS

Quantum mechanical methods, in particular methods based on density functional theory (DFT), can predict molecular structures of gas phase species with accuracy comparable to that of experimental methods. Predictions for transition metal oxides and other transition metal compounds are more difficult than main group compounds because partially filled d-shells and the weak coupling of d-electrons on different transition metal atoms lead to many nearly degenerate electronic states. Tests have shown (Pykavy, van Wüllen, & Sauer, 2004) that structures of the same quality as for main group compounds can be obtained for vanadium oxides if the B3LYP functional is used. For V–O bond dissociation energies, the hybrid B3LYP functional is superior to non-hybrid, gradient-corrected density functionals such as BLYP, BP86, or PBE (Sauer & Döbler, 2004). This is not necessarily true for other transition metal compounds as recently shown (Deglmann, Furche, & Ahlrichs, 2002). Comparison of IR-PD spectra with calculated IR spectra (see Section 4.6) provides evidence that only B3LYP correctly describes the size-depended localization of the extra electron in the $(V_2O_5)_n^-$ cage structures ($n = 2, 3, 4$), whereas BLYP predicts delocalization for all systems and BHLYP localization for all systems.

Density functional theory predictions for structures of vanadium oxide clusters of increasing size have first been made

for neutral clusters and cluster anions (Vyboishchikov & Sauer, 2000, 2001). For neutral V_4O_{10} clusters IR spectra have also been calculated (Vyboishchikov & Sauer, 2001), but comparison with the IR-MA spectrum (Beattie, Ogden, & Price, 1978) was not made. When IR-PD spectra became available for mono- and binuclear vanadium oxide cations (Asmis et al., 2004), B3LYP proved successful in reproducing them. The rms deviation was 13 and 26 cm^{-1} for the vanadyl (V=O) and V–O–V modes, respectively.

This level of agreement was achieved with different scale factors for the vanadyl modes (0.9167) and for the V–O–V modes as well as other modes below 900 cm^{-1} (0.9832). Scale factors are used to correct for systematic deviations of vibrational frequencies calculated within the harmonic approximation from observed fundamentals. Scaling accounts for anharmonicities which are negligible here (sizeable only for X–H bonds) and for systematic errors on the harmonic force constants calculated with a given quantum mechanical method. Although expansion of the database of safely assigned V–O frequencies may change the optimum scale factors (and increase somewhat the mean deviation), we apply the scale factors 0.9167 (V=O) and 0.9832 (V–O) to all simulated spectra shown in this work.

Calculation of harmonic vibrational frequencies profits very much from efficient codes for analytic evaluation of second energy derivatives such as implemented in TURBOMOLE for both closed shell and unrestricted open shell calculations (Deglmann, Furche, & Ahlrichs, 2002).

IV. VIBRATIONAL SPECTROSCOPY OF VANADIUM OXIDE IONS

An overview of the IR-PD spectra of vanadium oxide cations and anions is shown in Figures 3 and 4, respectively (Brümmer et al., 2003; Asmis et al., 2004; Gause, 2004; Asmis et al., 2005;

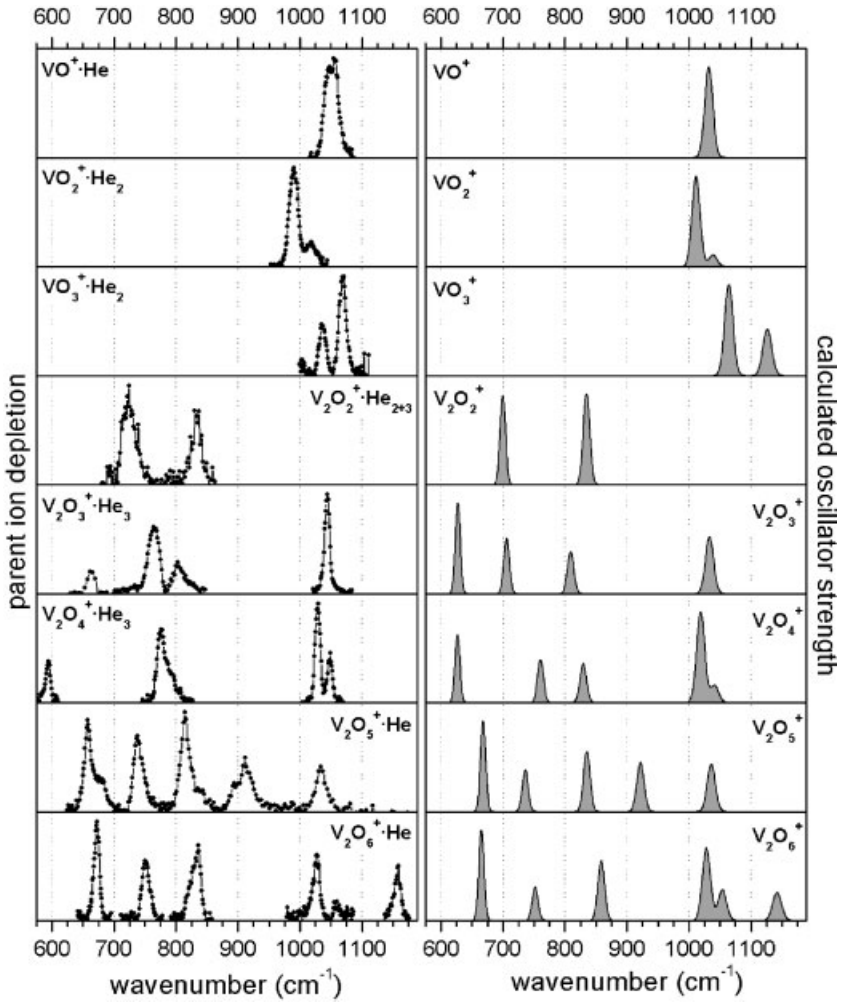

FIGURE 3. Overview of experimental IR-VPD spectra (**left column**) and simulated IR absorption spectra (**right column**), based on scaled B3LYP/TZVP frequencies and oscillator strengths of the lowest energy isomer in its electronic ground state of vanadium oxide cluster cations ranging from VO^+ to $V_2O_6^+$ (from **top** to **bottom**). Data from Ref. (Asmis et al., 2004).

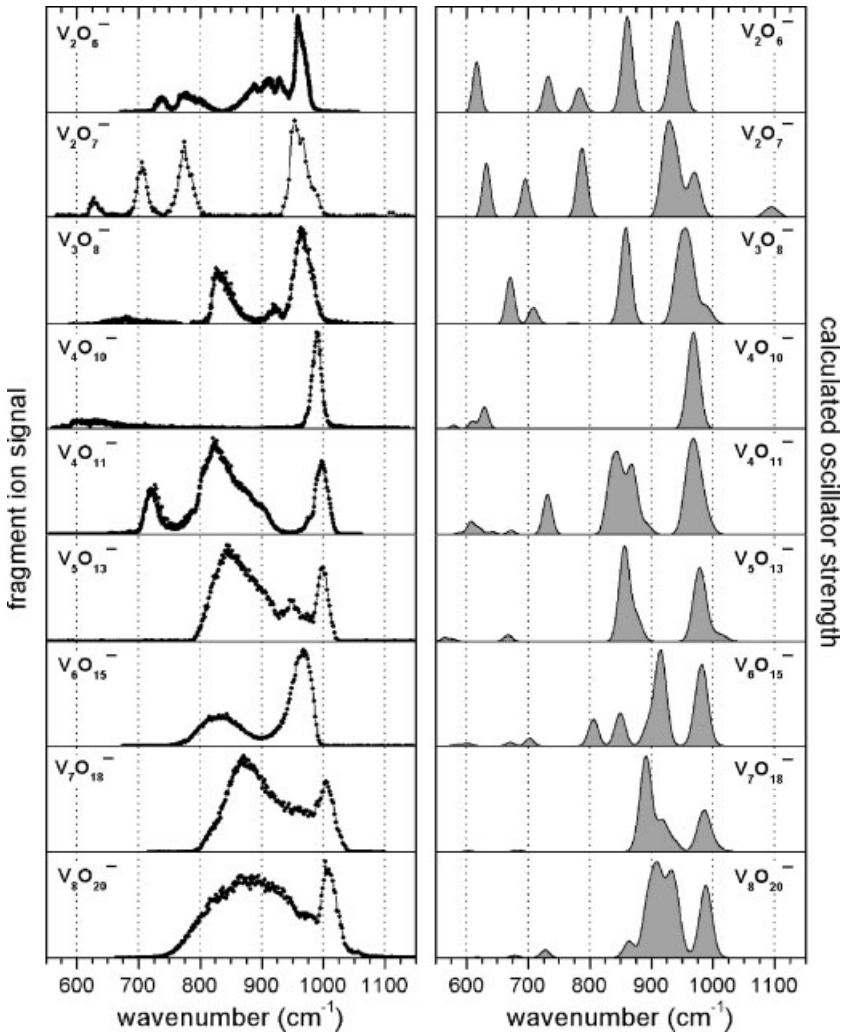

FIGURE 4. Overview of experimental IR-MPD spectra (**left column**) and simulated IR absorption spectra (**right column**), based on scaled B3LYP/TZVP frequencies and oscillator strengths of the lowest energy isomer in its electronic ground state of vanadium oxide cluster anions ranging from $V_2O_6^-$ to $V_8O_{20}^-$ (from **top** to **bottom**). From Ref. (Santambrogio et al., 2006).

Kaposta, 2005; Santambrogio et al., 2006). The experimental spectra (left) are shown together with the simulated spectra of the assigned isomers, which in most cases correspond to the lowest energy structure. Exceptions are discussed below. The geometric structures of the assigned isomers are shown in Figures 5 and 6.

A. Classification of Vibrational Modes

Three types of vibrational normal modes are active in the infrared spectra of vanadium oxide cluster ions (Fig. 7). (i) The vanadyl stretching region is located in-between 1,070 and 910 cm^{-1}. Typically, the vanadyl stretch modes lie below 1,000 cm^{-1} in the anions and above 1,000 cm^{-1} in the cations. (ii) Separated from and energetically below this region is the V–O–V stretching region, ranging from 870 cm^{-1} to below 600 cm^{-1} and mainly involving vibrational motion of the V–O single bonds comprising the ring and backbone structure of the cluster ions. Modes delocalized over larger parts of the ion are generally found at lower wave number. (iii) In oxygen-rich compounds various types of oxo-species can be observed, which range from associated O_2 molecules, over superoxo (O_2^-) to peroxo $(O_2)^{2-}$ species (the charges specified are formal charges). Because of an increasing occupation of anti-bonding π-orbitals, the bond order decreases with increasing formal negative charge. As a result, the O–O distance increases and the vibrational frequency is red-shifted. The originally dipole-forbidden vibrational transition (1,580 cm^{-1} in O_2) gains in intensity due asymmetric polarization of the electron cloud in the cluster. Table 2 shows some examples. In superoxo and peroxo species, the O–O distances are in the range of 1.29–1.35 Å and 1.41–1.47 Å, respectively, and the wave numbers in the range of 1,090–1,175 cm^{-1} and 875–975 cm^{-1}, respectively.

The intensities of the IR active modes range from weak, for example, ∼50 km/mol for the superoxo-mode in $V_2O_7^-$, to very strong (>2,000 km/mol) for individual O–V–O modes in the

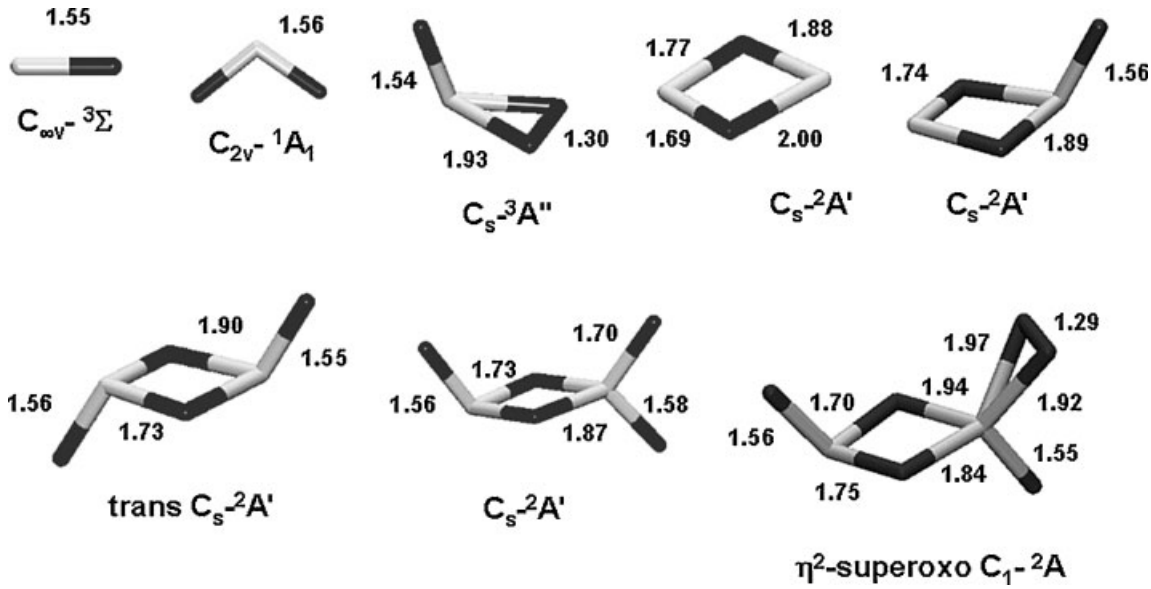

FIGURE 5. B3LYP/TZVP geometries and selected bond lengths for the lowest energy structures of vanadium oxide cations ranging from VO^+ (**top left**) to $V_2O_7^+$ (**bottom right**). The corresponding simulated infrared spectra are shown in Figure 3. Data from Ref. (Asmis et al., 2004).

largest cluster anions studied. In general, the intensity of the V–O–V modes is comparable to those of the V=O modes; however, since the latter often overlap in a narrower region, the vanadyl band is generally the most intense feature in the spectrum. An exception is $V_4O_{10}^-$, where the high symmetry of the cluster anion dominates the dipole selection rule, resulting in a comparably weak and red-shifted O–V–O band.

B. Assignment of Vibrational Spectra

The identification of the electronic state and geometric structure of a particular vanadium oxide cluster ion is based on the comparison between the experimental IR-PD spectra and simulated IR spectra of possible structural and electronic isomers. The simulated spectra are convoluted stick spectra, representing the scaled harmonic frequencies from B3LYP/TZVP calculations. An assignment based exclusively on the experiment or theory is nearly impossible for most vanadium oxides ions, because of the wealth of possible electronic states and structural isomers. Two examples are shown in Figure 8. For $V_2O_5^+$, the lowest two isomers are nearly identical with respect to their geometry, but differ in their electronic symmetry, $^2A'$ versus $^2A''$. Interestingly, their vibrational spectra are markedly different; five bands for the $^2A'$ isomer versus four bands for the $^2A''$ isomer. Comparison with the experiment nicely confirms the $^2A'$ isomer as the lowest in energy (Asmis et al., 2004), resolving a discrepancy in the literature concerning the nature of the electronic ground state of $V_2O_5^+$ (Calatayud, Andrés, & Beltrán, 2001; Justes et al., 2003b).

The $V_2O_6^+$ spectra (right side in Fig. 8) demonstrate the sensitivity of the vibrational spectra to the interaction with oxo-groups in oxygen-rich vanadium oxide ions. Isomer B had been suggested to be the ground state of $V_2O_6^+$ (Calatayud, Andrés, & Beltrán, 2001). Its vibrational spectrum, however, lacks a band observed in the experiment. This stimulated a further search, leading to isomer A which has a 46 kJ/mol lower energy. The two calculated isomers consist of a nearly identical trans-V_2O_4 unit, but differ in the way they bind the dioxygen group. Isomer A forms a η^2-superoxo structure, whereas isomer B only weakly binds the O_2 unit, forming an O_2-complex with formally no charge. The different types of binding are reflected in the scaled vibrational frequencies involving the O_2-unit: 1,142 cm^{-1} in the superoxo structure versus 1,404 cm^{-1} in the O_2 complex (Asmis et al., 2004). The experiment yields 1,160 cm^{-1}, confirming the superoxo structure.

C. Change in Structural Motifs with Cluster Size

Several structural motifs are found as a function of size. A characteristic four-membered planar V–O–V–O-ring is found in divanadium oxide cations (Asmis et al., 2004) and anions (Santambrogio et al., 2006). Its spectral signature consists of three in-plane deformation bands of comparable intensity in the 550–870 cm^{-1} region. Only two of these bands are observed for $V_2O_2^+$, because the third, predicted at 565 cm^{-1}, lies below the measurement window. An M(–O–)$_2$M (M = metal atom) ring was originally predicted for small neutral scandium oxide clusters (Johnson & Panas, 1999) and experimentally observed, in the form of a broad, unstructured band from 600 to 800 cm^{-1}, in the IR-REMPI spectra of neutral zirconium oxide clusters (von Helden et al., 2000). The latter study was not able to resolve the individual vibrational ring modes, mainly because of lack of mass selection of the absorbing (parent) species.

Vanadium oxide cluster ions with three vanadium atoms represent an intermediate cluster class; they show a three-

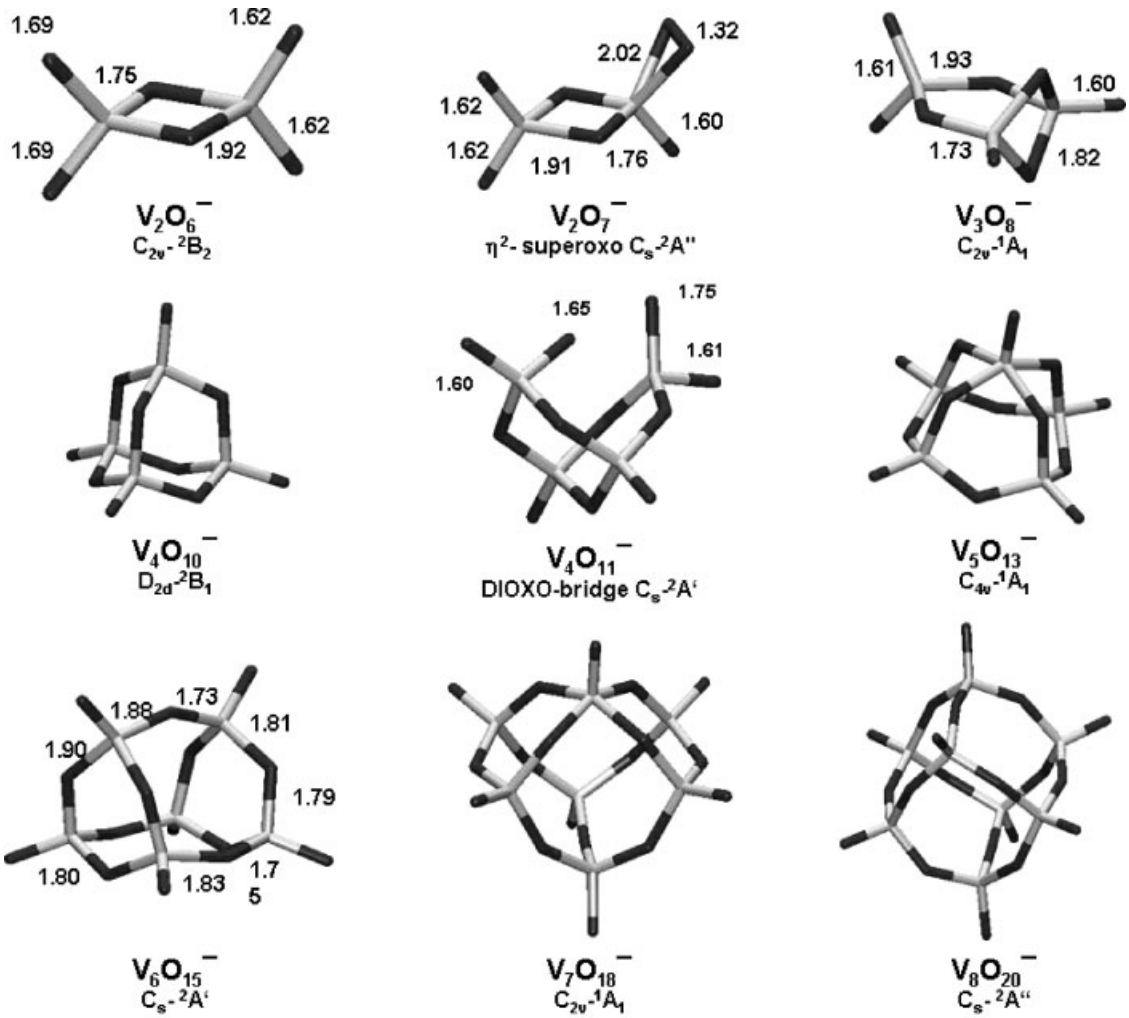

FIGURE 6. B3LYP/TZVP geometries and selected bond lengths for the lowest energy structures of vanadium oxide anions ranging from $V_2O_6^-$ (**top left**) to $V_8O_{20}^-$ (**bottom right**). The corresponding simulated infrared spectra are shown in Figure 4. Data from Ref. (Santambrogio et al., 2006).

dimensional backbone structure, but still contain one vanadium atom that contributes only two bonds to the cage backbone. $V_4O_{10}^-$ is the first cage structure in which each vanadium atom forms three V–O–V bonds and only a single terminal vanadyl bond. All larger clusters follow this trend, making the O=V(O–)$_3$ structural element and important feature of particular stable structure in $V_xO_y^{+/-}$ ions with $x \geq 4$.

Figure 9 compares the gas phase IR-MPD spectrum of $V_8O_{20}^-$ with the electron energy loss spectrum of a V_2O_5 surface (Tepper et al., 2002), which also probes vibrational states. The spectra are surprisingly similar in the region above 740 cm^{-1}, both displaying two bands of similar width and relative intensity. Their assignment is identical, that is, to vibrational modes of singly- and doubly-coordinated oxygen atoms. The third broad band of the surface spectrum is not observed in the gas phase. This can easily be rationalized, because this band is assigned (Clauws, Broeckx, & Vennik, 1985; Vyboishchikov & Sauer, 2001; Brázdová, Ganduglia-Pirovano, & Sauer, 2004) to triply coordinated oxygen sites, which do not exist in the $V_8O_{20}^-$ cluster anion. Hence, the vibrational spectra reflect clearly the common (V=O and V–O–V bonds) and the discriminating (triply coordinated O) structural features of gas phase clusters and solid surfaces.

D. Influence of cluster charge/number of electrons

Mass-selective IR-PD spectroscopy requires charged vanadium oxide species. For a given elemental composition, for example, V_4O_{10}, charged species are obtained by removal or addition of an electron. This may change the structure, properties, and reactivity of the species. Table 3 shows observed and calculated wave numbers for $V_4O_{10}^{+/0/-}$. With increasing number of electrons, the vanadyl vibrations shift to lower wave number, a trend that is well reproduced by the calculations. A shift to lower wave number is also seen for the V–O–V modes when passing from the cation to the neutral. In the anion, the delocalized additional

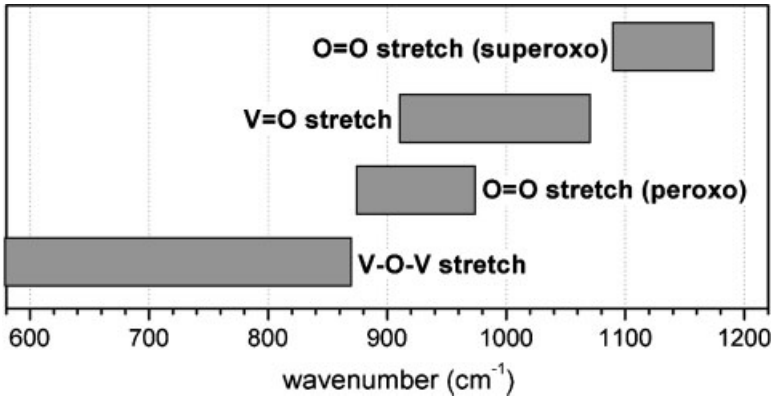

FIGURE 7. Energy ranges (in cm^{-1}) for the characteristic vibrational modes found in vanadium oxide cluster ions.

electron changes the V–O–V band qualitatively. Instead of an intense band around 200 cm^{-1} below the vanadyl band, a much less intense band is observed around 320–390 cm^{-1} below the vanadyl band. This change has its origin in the delocalization of the additional electron over d-states of the four V sites in $V_4O_{10}^-$ (see below, Section 4.6)

The observed IR-PD spectrum of the (radical) cation (not shown) (Asmis et al., 2002) is very similar to that of the neutral V_4O_{10} cluster and does not show any indication of a major structural change compared to the neutral species (Sauer & Döbler, 2004; Feyel, Schröder, & Schwarz, 2006). Removal of an electron from the π-bonding orbital of the vanadyl bond

TABLE 2. Calculated O–O Bond Length (in Å), as well as Calculated and Observed Frequencies (in cm^{-1}) for O–O Stretch Vibrations in Superoxo and Peroxo Groups Compared to O_2

Type		Calcd[a] R_{OO}	Calcd[a] ν_{OO}	Obsd ν_{OO}
Molecule	$^3O_2$ gas phase	1.21	1524	1556
η^2-Superoxo	$V_2O_6^+$	1.29	1175	1160
	VO_4 matrix	1.31	1129	1122[f]
η^1-Superoxo	$V_2O_7^-$	1.31	1138	1112
Superoxo	$^2O_2^-$ gas phase	1.35	1102	1090[e]
η^2-Peroxo	$O_2VSi_7O_{12}H_7$ [b]	1.43[b]	984[b]	(951)[c]
	V_4O_{11}	1.41	957	(951)[c]
	$VO(O_2)(C_2O_4)_2^{3-}$	(1.43)[d]		904[d]
Peroxo	H_2O_2	1.47	886	878

[a]B3LYP functional/TZVP basis set, scale factor 0.9429, see Asmis et al. (2004).

[b](Pritzsche, Döbler, & Sauer, unpublished work).

[c]Obsd. for peroxo species on V_2O_3(0001) surface, (Abu Haija et al., 2006).

[d]Distance obsd., see Ref. (Reynolds & Butler, 1996) for references to the original work.

[e]Estimated from experimental data for LiO_2 and NaO_2 for O_2^- well separated from counterion, (Cramer et al., 2003).

[f](Chertihin, Bare, & Andrews, 1997).

creates a single bond with an unpaired electron on oxygen, $V{=}O \rightarrow V^{(+)} - O^{\cdot} + e^{-}$,

SOMO of $V_4O_{10}^{+}$

which is highly reactive and abstracts a hydrogen atom even from methane (Feyel, Schröder, & Schwarz, 2006). The localization of the hole in the cation (see the singly occupied orbital above) as opposed to the delocalization of the additional electron in the anion (see SONO(1) in Section 4.6) is explained by the different nature of the HOMO and LUMO in V_4O_{10}, O-2p orbitals in the former, and V-3d orbitals in the latter case. The $V^{(+)}$–$O^{\cdot}$ bond is much longer (1.75 Å) than the three other vanadyl bonds (1.56 Å) and, hence, its stretch vibration is shifted to lower wave number. It is predicted to occur around 720 cm^{-1} (scaled by 0.9832), below the V–O–V band. Its vanishing intensity explains why such a band is not seen in the IR-PD spectrum of $V_4O_{10}^{+}$. Without having done the DFT calculations, one would conclude that the structures of V_4O_{10} and $V_4O_{10}^{+}$ are very similar. This is another example illustrating the importance of a combination of experiment and computation in this field.

E. Influence of the Messenger Atom

When a He atom is used as a messenger in the vibrational predissociation measurements, it is generally assumed that its influence on the cluster ion energetics and dynamics is negligible. This is supported by experiments (Brümmer et al., 2003) and high-level calculations (Döbler & Sauer, Private communication; Kaposta, 2005) which have been performed on VO^{+} complexes with various messenger atoms/molecules. Experimentally, we find $1{,}053 \pm 5$ cm^{-1} for the He atom messenger complex (see Fig. 10) and small relative shifts (± 1 cm^{-1}) for the $VO^{+}{\cdot}He_n$ ($n > 1$) and $VO^{+}{\cdot}He_2$ complexes. The CASPT2/cc-pVQZ harmonic frequencies of VO^{+} and $VO^{+}{\cdot}He$ are 1,052 and 1,054 cm^{-1}, respectively, in excellent agreement with the experimental values. An Ar atom, on the other hand, may cause complications (Fielicke et al., 2005; Walker et al., 2005; Fielicke, Rabin, & Meijer, 2006), because of its eight times larger polarizability, which leads to a considerably stronger charge–induced dipole interaction with the ion. For an Ar atom, the experimentally observed shift is $+8$ cm^{-1}, significantly larger than that for He. However, the fact that the binding energy of an Ar atom to VO^{+} is more than four times larger ($D_e = 3{,}535$ cm^{-1}) compared to $VO^{+}{\cdot}He$ ($D_e = 788$ cm^{-1}) presents a more problematic situation. Excitation of a single quantum of the V=O stretch vibration is

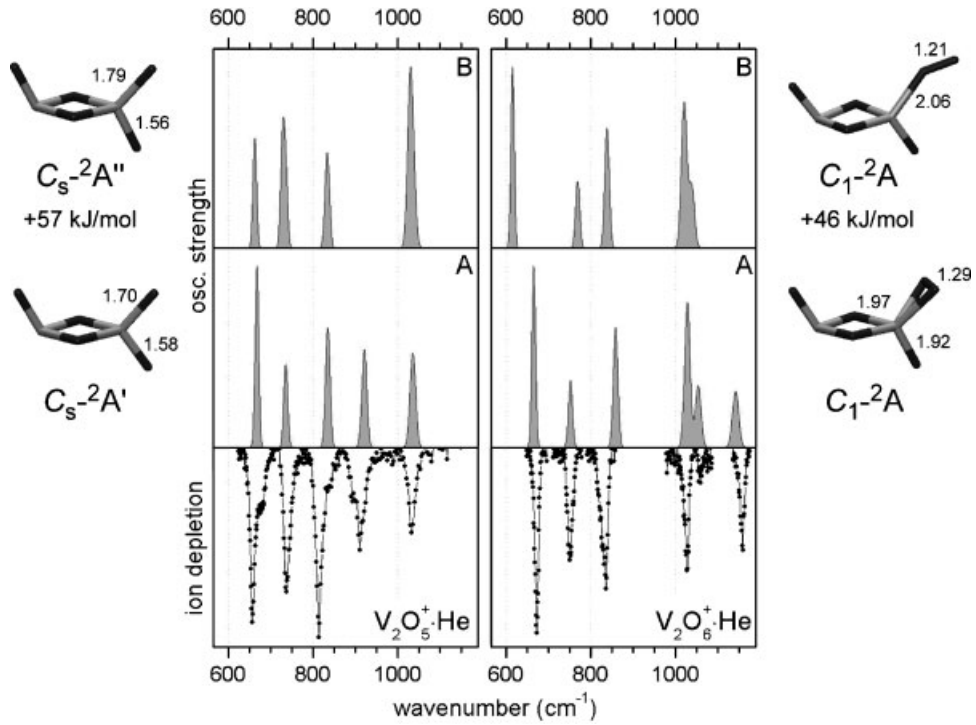

FIGURE 8. Assignment of the experimental vibrational spectra based on comparison with simulated IR spectra. The experimental IR-VPD spectra of $V_2O_5^{+}{\cdot}He$ (**bottom left**) and $V_2O_6^{+}{\cdot}He$ (**bottom right**) are shown together with the lowest (**A**) and second lowest (**B**) energy isomers of $V_2O_5^{+}$ (left) and $V_2O_6^{+}$ (right).

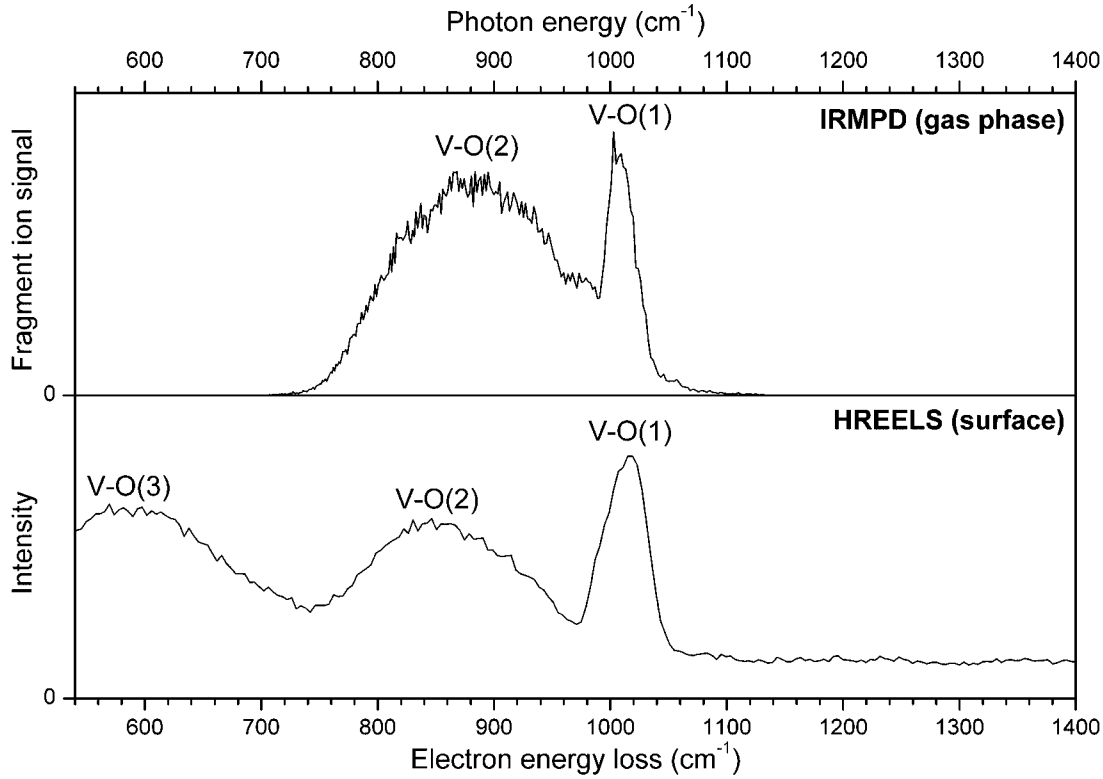

FIGURE 9. Vibrational spectra of different forms of vanadium oxide. The IRMPD spectrum of the gas phase cluster anion $V_8O_{20}^-$ (**top**) and the spectrum of a freshly cleaved 001 surface of V_2O_5 (**bottom**), measured using high-resolution electron energy loss spectroscopy (Tepper et al., 2002) are shown.

thus sufficient to overcome the predissociation threshold in VO^+·He, whereas excitation of at least four quanta is required for the VO^+·Ar complex.

The IR-PD spectra of $V_3O_6^+$·Ar_2 (see Fig. 11) and $V_3O_7^+$·Ar (see Fig. 12) are two instructive examples for the non-negligible influence of the messenger atom when Ar is used. The lowest energy structure found for $V_3O_6^+$ is the chain-like structure shown in Figure 11. Its scaled harmonic frequencies (spectrum C) line up with the experimentally observed bands rather well; better than, for example, the frequencies of the energetically second lowest isomer (spectrum D), which is characterized by a ribbon-like structure. However, the experimental spectrum reveals additional bands in the V–O–V stretch region that spectrum C does not reproduce. Calculations on the Ar-complexes of $V_3O_6^+$ confirm (spectra A and B) that the additional bands are, at least in part, due to a splitting of the vibrational modes as a result of the asymmetric solvation of $V_3O_6^+$ by the Ar atoms. The discrepancy with respect to the intensity of the vanadyl band relative to the V–O–V bands between the experimental spectrum and spectrum C probably results from the high-binding energy for the second Ar atom of 21.3 kJ/mol, respectively. Consequently, the absorption of at least two, and in the region below ~900 cm^{-1}, at least three IR photons is required to overcome the pre-dissociation threshold in $V_3O_6^+$·Ar_2.

A different situation is found for $V_3O_7^+$ (see Fig. 12). Here, the calculations on bare $V_3O_7^+$ find a caged structure lowest in energy, but its IR spectrum disagrees with the experimental spectrum of $V_3O_7^+$·Ar (Fig. 12). Interestingly, the simulated IR spectra of the (bare) ring isomer found 17.4 kJ/mol above the (bare) caged isomer matches much better. Calculations on the respective Ar complexes yield almost identical IR spectra (e.g., spectrum A and B in Fig. 12), but, surprisingly, change the energetic ordering of the isomers. While the Ar complex of the cage isomer is only stabilized by 15.6 kJ/mol relative to the bare ion, the ring isomer is found to drop by 50.1 kJ/mol in energy, placing it 17.1 kJ/mol below (!) the Ar complex of cage isomer. This behavior is exceptional, but emphasizes the importance of taking the influence of the Ar atom into account.

F. Electron Localization

Symmetry-breaking electron or hole localization is observed in many chemical systems and its proper description by DFT depends on the functional used. For example, the electron hole created in quartz when doped with Al is not delocalized over all four oxygen sites of the AlO_4 defect site, but localized at one oxygen only (Pacchioni et al., 2001; Solans-Monfort et al., 2004). We use the measured IR-MPD spectra of $(V_2O_5)_n^-$ with $n = 2$, 3, and 4 as the criterion for selecting the proper functional and find that only B3LYP has the right admixture of Fock exchange to reproduce the size-dependent change from delocalized to

TABLE 3. Calculated and Observed Vibrational Frequencies (in cm^{-1}) for the Negative Ion, Neutral Species and Positive Ion of V_4O_{10}

system	Symmetry	Experiment[a] V=O stretch	V-O-V	B3LYP (scaled) V=O stretch	V-O-V
$V_4O_{10}^+$	$^2A''$ (C_s)	1034	839	1038	861
V_4O_{10}	(T_d)	1030	828	1010	839
$V_4O_{10}^-$	(D_{2d})	990	670/637/602	969	629/609

[a](Beattie, Ogden, & Price, 1978; Asmis et al., 2002; Santambrogio et al., 2006).

localized d-electron states in vanadium oxide cages correctly (Asmis et al., 2005).

SONO(1) **SONO(2)** **SONO(3)**

For $V_4O_{10}^-$, we find a tetragonal D_{2d} structure which is minimally Jahn–Teller distorted from the T_d structure. The unpaired electron is completely delocalized over d-states of all four vanadium sites as illustrated by its singly occupied natural orbital **SONO(1)**. In contrast, in the larger anions the unpaired electron localizes at a single vanadium site, which lowers the symmetry of their structures to C_s. For $V_6O_{15}^-$ and $V_8O_{20}^-$ we find the distorted trigonal prism and cube structures (Fig. 6). Their singly occupied natural orbitals, **SONO(2)** and **SONO(3)**, reflect the localization of the unpaired electron. Unlike the closed-shell neutral parent compounds, the D_{3h} structure (trigonal prism) of $V_6O_{15}^-$ and the D_{2d} structure (cube) of $V_8O_{20}^-$ are higher order saddle points. For both $V_6O_{15}^-$ and $V_8O_{20}^-$ first order saddle points with C_{2v} symmetry are found, which represent transition structures for the interconversion of two equivalent C_s-minimum structures and have the additional electron delocalized over two sites.

The effects of symmetry breaking are directly observed in the vibrational spectra of these species, indicated by the gray-shaded area in Figure 13. Upon localization of the unpaired electron intense V–O–V, stretch transitions appear ~100–200 cm^{-1} below the strong vanadyl band, which replace the weak V–O–V feature more than ~350 cm^{-1} below the vanadyl

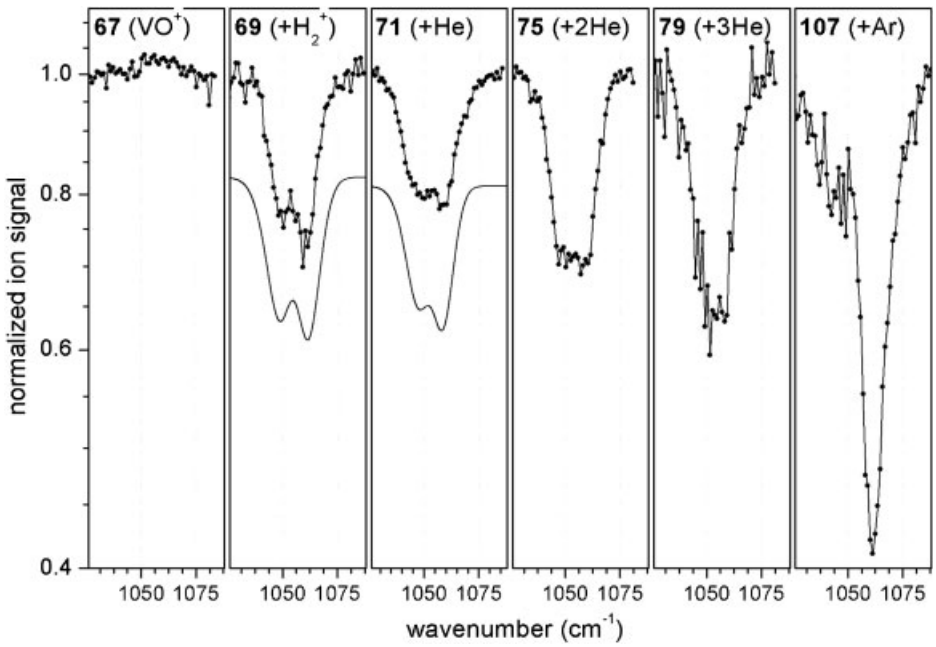

FIGURE 10. IR-PD spectra (solid dots) measured by monitoring the yield of VO^+ (67 amu) and $VO^+ \cdot X$ ($X = H_2$, He, He_2, He_3, and Ar) in the region of the fundamental of the $^3\Sigma^-$ ground state of VO^+. Lines are shown to aid the eye. Simulated spectra (solid lines) are also shown, vertically displaced, for H_2–VO^+ and He–VO^+. The double minimum feature is attributed to rotational resolved structure.

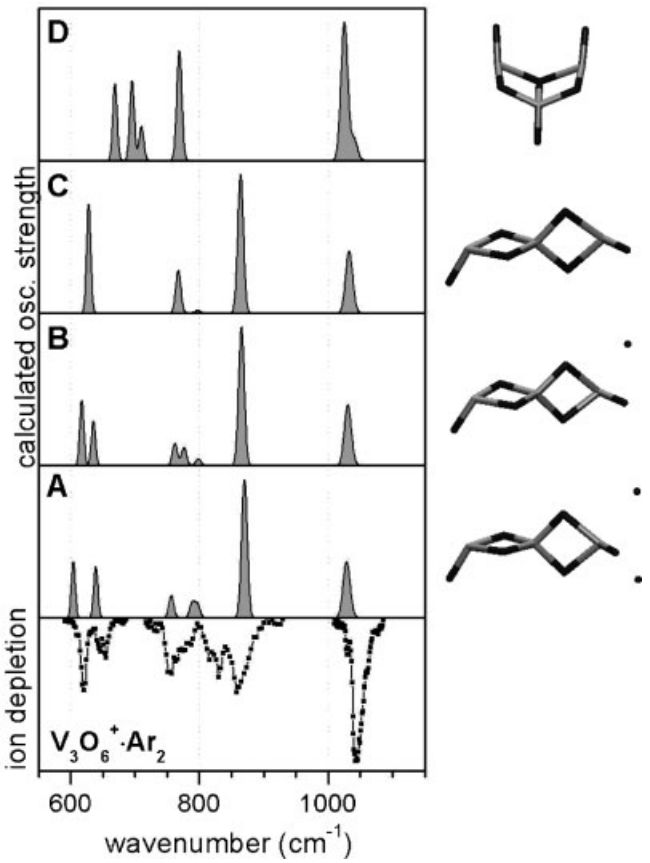

FIGURE 11. Experimental IR-VPD spectrum of $V_3O_6^+ \cdot Ar_2$ (**bottom**) and four (**A**–**D**) simulated IR spectra. The two spectra at the top correspond to the two lowest energy isomers of (bare) $V_3O_6^+$ with chain-like (**C**) and ribbon-like (**D**) geometries (spectrum D), respectively. For the chain-like isomer the IR spectra of the corresponding messenger atom complexes with one (spectrum B) and two Ar atoms (spectrum A) are also shown.

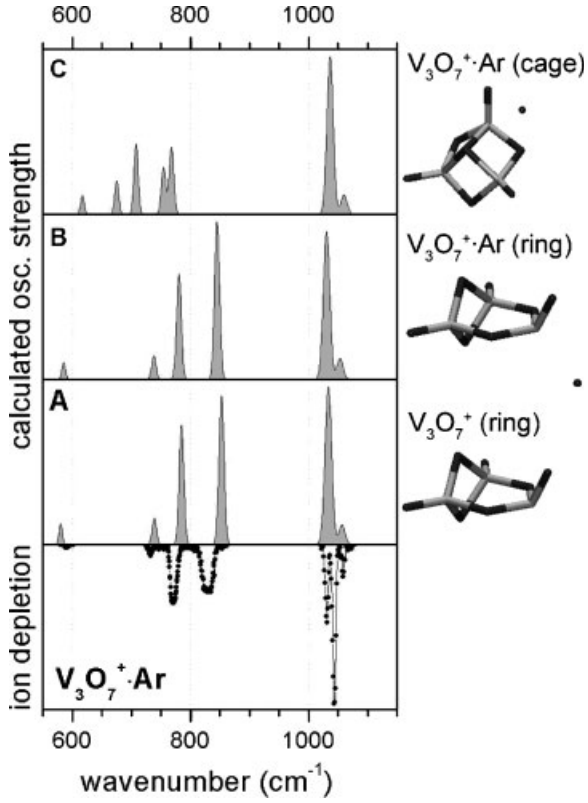

FIGURE 12. The experimental IR-VPD spectrum of $V_3O_7^+ \cdot Ar$ (bottom) and the simulated IR spectra of the Ar messenger atom complexes of the two lowest energy isomers with ring-like (**B**) and a cage-like geometries (**C**), respectively. The simualted IR spectrum of the bare ring-like isomer is also shown (**A**).

band in the spectrum of the delocalized case ($V_4O_{10}^-$). The vanadyl modes are not affected by the electron localization and therefore their position and width remain nearly unchanged. Comparison with the experimental infrared spectra confirms the general predictions of the B3LYP model, in particular the pronounced, qualitative changes upon electron localization when the size of the cluster is increased.

Figure 13 shows not only the B3LYP results discussed so far, but also results of DFT calculations which employ the BLYP (Becke, 1988; Lee, Yang, & Parr, 1988) and BHLYP (Lee, Yang, & Parr, 1988; Becke, 1993) functionals. The increasing admixture of Fock exchange (zero, 20 and 50%) in BLYP, B3LYP, and BHLYP, respectively, leads to an increasing tendency for symmetry breaking (Pacchioni et al., 2001; Sherrill, Lee, & Head-Gordon, 1999; Sodupe et al., 1999; Solans-Monfort et al., 2004). BHLYP (right column in Fig. 13) yields localization of the unpaired electron for all three cage-type anions, also for $V_4O_{10}^-$. Consequently, the BHLYP spectrum of $V_4O_{10}^-$ shows additional bands between 800 and 900 cm^{-1} that are absent in the experimental spectrum. In contrast, BLYP predicts delocalization of the unpaired electron for all three cage-type anions studied and C_{2v} and D_{2d} structures become the ground states of $V_6O_{15}^-$ and $V_8O_{20}^-$, respectively. All three BLYP spectra do not show any band between 750 and 950 cm^{-1}, which is in clear contrast with the experimental spectra of $V_6O_{15}^-$ and $V_8O_{20}^-$. In summary, Figure 1 shows that only B3LYP reproduces correctly the transition from symmetric (delocalized) to broken-symmetry (localized) structures when passing from $V_4O_{10}^-$ to $V_6O_{15}^-$ in this series of $(V_2O_5)_n^-$ cluster anions.

This conclusion is further supported by single point CCSD(T) calculations which have been made on the BHLYP optimized structures (Santambrogio et al., 2006). They confirm that for $V_4O_{10}^-$ the D_{2d} structure has a lower energy than the C_s structure (33 kJ/mol compared to 7 kJ/mol with B3LYP), whereas for $V_6O_{15}^-$ the C_{2v} structure has a higher energy than the C_s structure (9 kJ/mol compared to 10 kJ/mol with B3LYP).

V. OUTLOOK

We conclude this review by highlighting several recent advances that may have a significant impact on the presented research field; these include:

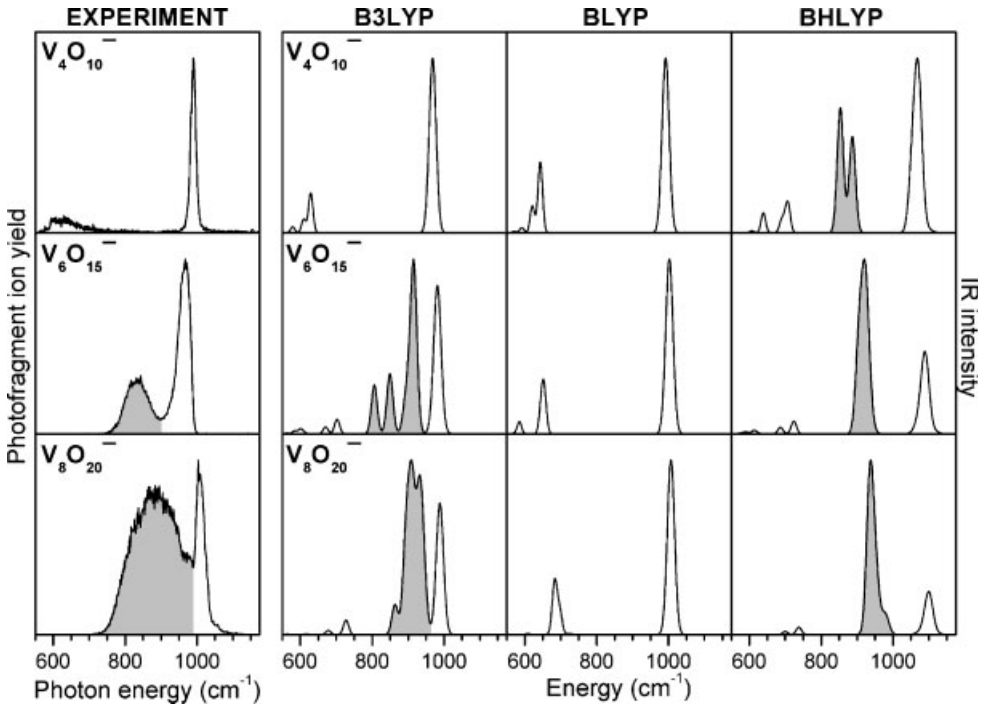

FIGURE 13. Experimental and simulated vibrational spectra of vanadium oxide cluster anions in the region of the V–O single and double bond stretch modes. IRMPD spectra (**left**) of $V_4O_{10}^-$ (**top**), $V_6O_{15}^-$ (**center**) and $V_8O_{20}^-$ (**bottom**) were measured from 550 to 1175 cm^{-1} monitoring the dominant fragmentation channel, leading to formation of $V_3O_8^-$, $V_4O_{10}^-$, and $V_4O_{10}^-$, respectively. Simulated spectra (**right**) were obtained from scaled harmonic frequencies and oscillator strengths employing the B3LYP, BLYP, and BHLYP functionals. The calculated stick spectra were convoluted for better comparison with the experiment. Gray-shaded peaks indicate localization of the unpaired d-electron.

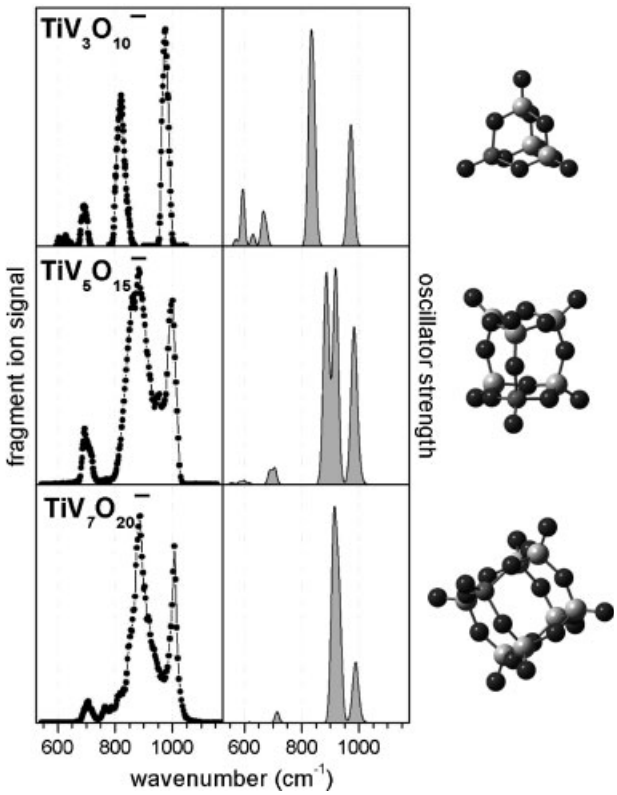

(i) improved, table top IR laser systems;
(ii) new, more flexible ion sources; and
(iii) genetic algorithms for finding global minimum structures.

Because of the limited access to FEL facilities, a relatively small number of IR-PD experiments on mass-selected clusters ions have been performed over the last decade. Recent advances in the technology of intense and tunable mid-IR lasers may soon change this. One approach is based on difference frequency mixing in an $AgGaSe_2$ crystal, pioneered by Raffy et al. (1994) and considerably improved and first applied to gas phase spectroscopy by Gerhards and co-workers (Gerhards, 2004; Gerhards, Unterberg, & Gerlach, 2002). The three stage system consists of a tunable near IR laser (3,650–4,000 cm^{-1}, bandwidth 0.04 cm^{-1}), whose output is amplified in a $LiNbO_3$ based OPA. The signal and idler of the OPA process are then used for difference-frequency mixing in an $AgGaSe_2$ crystal, leading to tunable radiation from 2,100 to 1,400 cm^{-1} with a pulse energy of $\sim$1 mJ at 1,645 cm^{-1} and a bandwidth of 0.1 cm^{-1}. Bosenberg and Guyer (1993) have used the same type of crystal, but a more complex OPO/OPA setup, to achieve similar specifications.

FIGURE 14. Experimental IR-MPD and simulated B3LYP/TZVP IR spectra of the monosubstituted $TiV_{2x+1}O_{5(x+1)}^-$ anions with $x = 1, 2$, and 3. The corresponding geometries (oxygen: dark, titanium: gray, and vanadium: light gray) are shown on the right.

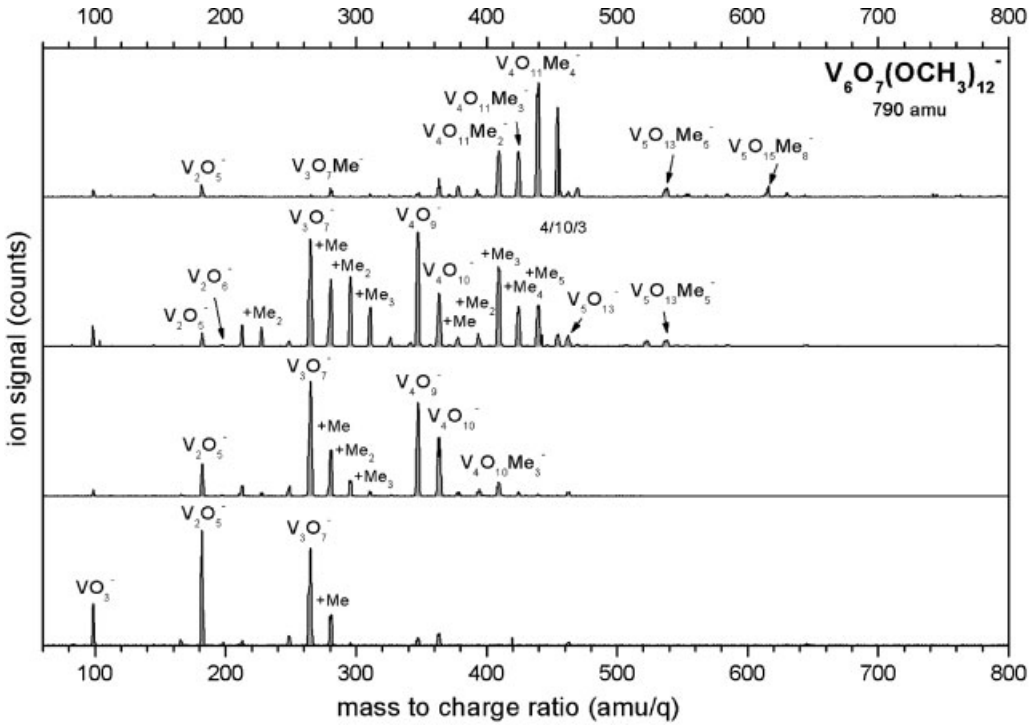

FIGURE 15. Ion distribution of vanadium oxide containing anions produced by ion spraying a methanol solution containing the hexanuclear methoxo-oxovanadium cluster V_6O_7 $(OCH_3)_{12}$ as a precursor. The degree of fragmenation can be controlled by changing the source parameters (**top**: mild conditions; **bottom**: harsh conditions).

Johnson and co-workers have recently used a Laser Vision KTP/KTA/AgGaSe2 optical parametric oscillator/amplifier system to measure IR spectra in the range from 600 to 1,900 cm^{-1} (Headrick, Bopp, & Johnson, 2004; Diken et al., 2005), convincingly demonstrating that the fingerprint region is now accessible to IR-PD experiments of weakly bound species. An alternate continuously tunable, narrow bandwidth (0.4 cm^{-1}) laboratory laser source for the mid-IR spectral range of 1,250–2,270 cm^{-1} has been developed by Vilesov and co-workers (Kuyanov, Momose, & Vilesov, 2004). The device is based on the stimulated backward Raman scattering in solid para-hydrogen at 4 K. The crystal is pumped by a focused beam obtained from a commercial near-IR OPO. Output energies range from 1.7 mJ at 2,270 cm^{-1} to 120 μJ at 1,250 cm^{-1}.

Advances with respect to cluster ion sources are aimed at a greater flexibility in producing the metal oxide species. Recently, the first IR-MPD spectra of mixed metal oxide clusters were measured (Janssens et al., 2006), using a dual laser dual metal target laser vaporization source (Fig. 14). Adding a second metal to clusters allows both the electronic and geometric structure of the cluster ion to be tailored. By looking at singly substituted $TiV_{y-1}O_z^-$ cluster anions, for example, the structure of the isoelectronic neutral, pure V_yO_z cluster can be probed. These experiments are aimed at eventually producing model systems in the gas phase that simulate the metal oxide cluster–metal oxide support interaction. Other promising approaches include measuring IR-MPD spectra of vanadium oxide ion–hydrocarbon complexes (Fielicke et al., 2003) and the application of ion spray techniques to the production of gas phase vanadium oxide ions (Feyel, Schröder, & Schwarz, 2006). Feyel et al., for example, recently demonstrated the efficient gas phase production of vanadium oxide ions (see Figure 15) from a methanol solution containing the hexanuclear methoxo-oxovanadium cluster V_6O_7 $(OCH_3)_{12}$ as a precursor.

On the computational side, there are several new global optimization strategies that all aim at generating most different starting structures including unusual bonding situations. Monte Carlo techniques may be used to generate an ensemble of starting structures or simulated annealing may be used to sample waste regions of the potential energy surface. The most promising approach is implementation of a genetic algorithm that finds the global minimum structure by an evolutionary process (Deaven & Ho, 1995). Some of the candidate structures are selected as parents to obtain the next generation by mating or mutations. The relative energy is used as fitness parameter. For the $V_4O_{11}^-$ case, chemical intuition had lead to the μ-(η^2:η^2)-peroxo structure, structure B shown in Figure 16 (Santambrogio et al., 2007). However, the calculated spectrum was not in sufficient agreement with the observed one (Fig. 16). Application of a genetic algorithm implemented by M. Sierka (Sierka et al., 2007) on the basis of Deaven and Ho (1995) produced additional structures. The lowest energy structure found by the genetic algorithm shows the dioxo motif at two vanadium sites (structure A in Fig. 16). The IR spectrum calculated for this structure shows the best agreement with the observed IR spectrum. Although this approach is much more expensive than

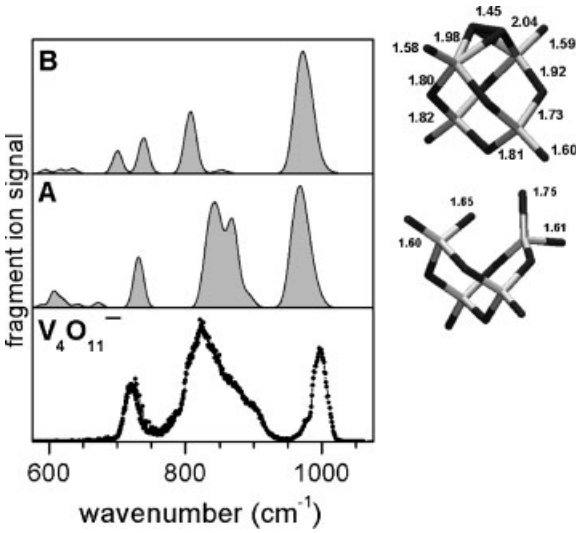

FIGURE 16. The experimental IR-MPD spectrum of $V_4O_{11}^-$ (**bottom**), two simulated IR spectra (**A** and **B**) of two energetically low-lying $V_4O_{11}^-$ isomers and their corresponding structures (**right**). Bond lengths are given in Å.

chemical "intuition," it will play an increasing role in the structure determination of clusters. Here, chemical intuition faces limits because clusters represent chemical compounds under unusual conditions.

ACKNOWLEDGMENTS

We gratefully acknowledge the contributions from all authors of the original papers, namely M. Brümmer, J. Döbler, O. Gause, E. Janssens, C. Kaposta, G. Meijer, K. Rademann, G. Santambrogio, G. von Helden, and L. Wöste. This work is supported by the Collaborative Research Center 546 of the Deutsche Forschungsgemeinschaft. J. Sauer thanks M. Sierka for providing the genetic algorithm prior to publication. K. Asmis gratefully acknowledges the support of the Stichting voor Fundamenteel Onderzoek der Materie (FOM) in providing the required beam time on FELIX and highly appreciate the skillful assistance of the FELIX staff.

REFERENCES

Abu Haija M, Guimond S, Romanyshyn Y, Uhl A, Kuhlenbeck H, Todorova TK, Ganduglia-Pirovano MV, Döbler J, Sauer J, Freund H-J. 2006. Low temperature adsorption of oxygen on reduced V_2O_3(0 0 0 1) surfaces. Surf Sci 600:1497–1503.

Asmis KR, Brümmer M, Kaposta C, Santambrogio G, von Helden G, Meijer G, Rademann K, Wöste L. 2002. Mass-selected infrared photodissociation spectroscopy of $V_4O_{10}^+$. Phys Chem Chem Phys 4:1101–1104.

Asmis KR, Meijer G, Brümmer M, Kaposta C, Santambrogio G, Wöste L, Sauer J. 2004. Gas phase infrared spectroscopy of mono- and divanadium oxide cluster cations. J Chem Phys 120:6461–6470.

Asmis KR, Santambrogio G, Brümmer M, Sauer J. 2005. Polyhedral vanadium oxide cages: Infrared spectra of cluster anions and size-induced d-electron localization. Angew Chem Int Ed 44:3122–3125.

Beattie IR, Ogden JS, Price DD. 1978. Characterization of molecular V_4O_{10}, an analog of P_4O_{10}. Inorg Chem 17:3296–3297.

Becke AD. 1988. Density-functional exchange-energy approximation with correct asymptotic-behavior. Phys Rev A 38:3098–3100.

Becke AD. 1993. A new mixing of hartree-fock and local density-funtional theories. J Chem Phys 98:1372–1377.

Bell RC, Castleman AW Jr. 2002. Reactions of vanadium oxide cluster ions with 1,3-butadiene and isomers of butene. J Phys Chem A 106:9893–9899.

Bell RC, Zemski KA, Castleman AW Jr. 1998. Gas-phase chemistry of vandium oxide cluster cations. 1. Reactions with C_2F_6 and CH_3CF_3. J Phys Chem A 102:8293–8299.

Bell RC, Zemski KA, Kerns KP, Deng HT, Castlemann AW Jr. 1998b. Reactivities and collision-induced dissociation of vanadium oxide cluster cations. J Phys Chem A 102:1733–1742.

Bell RC, Zemski KA, Castleman AW Jr. 1999a. Gas-phase chemistry of vanadium oxide cluster cations 3. Reactions with CCl_4. J Phys Chem A 103:1585–1591.

Bell RC, Zemski KA, Castleman AW Jr. 1999b. Gas phase chemistry of vandium oxide cluster cations. 2. Reactions with CH_2F_2. J Phys Chem A 103:2992–2998.

Bell RC, Zemski KA, Castleman AW Jr. 1999c. Size-specific reactivities of vanadium oxide cluster cations. J Cluster Sci 10:509–524.

Bell RC, Zemski KA, Justes DR, Castleman AW Jr. 2001. Formation, structure and bond dissociation thresholds of gas-phase vanadium oxide cluster ions. J Chem Phys 114:798–811.

Berkowitz J, Chupka WA, Inghram MG. 1957. Thermodynamics of the V–O system—Dissociation energies of VO and VO_2. J Chem Phys 27:87–90.

Bieske EJ, Dopfer O. 2000. High resolution spectroscopy of cluster ions. Chem Rev 100:3963–3998.

Black JG, Yablonovitch E, Bloembergen N, Mukamel S. 1977. Collisionless multiphoton dissociation of S F_6: A statistical thermodynamic process. Phys Rev Lett 38:1131–1134.

Böhme DK, Schwarz H. 2005. Gas-phase catalysis by atomic and cluster metal ions: The ultimate single-site catalysts. Angew Chem Int Ed 44: 2336–2354.

Bosenberg WR, Guyer DR. 1993. Broadly tunable, single-frequency optical parametric frequency conversion system. J Opt Soc Am Soc B 10:1716–1722.

Brázdová V, Ganduglia-Pirovano MV, Sauer J. 2004. Periodic density functional study on structural and vibrational properties of vanadium oxide aggregates. Phys Rev B 69:165420–16542014.

Brümmer M, Kaposta C, Santambrogio G, Asmis KR. 2003. Formation and photodepletion of cluster ion—Messenger atom complexes in a cold ion trap: Infrared spectroscopy of VO^+, VO_2^+ and VO_3^+. J Chem Phys 119:12700–12703.

Calatayud M, Andrés J, Beltrán A. 2001. A systematic density functional theory study of $V_xO_y^+$ and V_xO_y (x = 2–4, y = 2–10) systems. J Phys Chem A 105:9760–9775.

Calatayud M, Silvi B, Andrés J, Beltrán A. 2001b. A theoretical study on the structure, energetics, and bonding of VO_x^+ and VO_x (x = 1–4) systems. Chem Phys Lett 333:493–503.

Chertihin GV, Bare WD, Andrews L. 1997. Reactions of laser-ablated vandium atoms with dioxygen. Infrared spectra of VO, VO_2, $OOVO_2$, and V_2O_2 in solid argon. J Phys Chem A 101:5090–5096.

Clauws P, Broeckx J, Vennik J. 1985. Lattice-vibrations of V_2O_5—Calculation of normal vibrations in a urey-bradley force-field. Phys Status Solidi B 131:459–473.

Cramer CJ, Tolman WB, Theopold KH, Rheingold AL. 2003. Variable character of O–O and M–O bonding in side-on (eta(2)) 1:1 metal complexes of O-2 PNA. 100:3635–3640.

Davis S, Fárník M, Uy D, Nesbitt DJ. 2001. Concentration modulation spectroscopy with a pulsed slit supersonic discharge expansion source. Chem Phys Lett 344:23–30.

de Almeida LAL, Deep GS, Lima AMN, Khrebtov IA, Malyarov VG, Neff H. 2004. Modeling and performance of vanadium–oxide transition edge microbolometers. Appl Phys Lett 85:3605–3607.

Deaven DM, Ho KM. 1995. Molecular-geometry optimization with a genetic algorithm. Phys Rev Lett 75:288–291.

Deglmann P, Furche F, Ahlrichs R. 2002. An efficient implementation of second analytical derivatives for density functional methods. Chem Phys Lett 362:511–518.

Dietz TG, Duncan MA, Powers DE, Smalley RE. 1981. Laser production of supersonic metal cluster beams. J Chem Phys 74:6511–6512.

Diken EG, Headrick JM, Roscioli JR, Bopp JC, Johnson MA, McCoy AB. 2005. Fundamental excitations of the shared proton in the $H_3O_2^-$ and $H_5O_2^+$ complexes. J Phys Chem A 109:1487–1490.

Dinca A, Davis TP, Fisher KJ, Smith DR, Willett GD. 1999. Vanadium oxide anion cluster reactions with methyl isobutyrate and methyl methacrylate monomer and dimer: A study by FT/ICR mass spectrometry. Int J Mass Spectrom 182/183:73–84.

Duncan MA. 2000. Frontiers in the spectroscopy of mass-selected molecular ions. Int J Mass Spectrom 200:545–569.

Dyke JM, Gravenor BWJ, Hastings MP, Morris A. 1985. High-temperature photoelectron spectroscopy: The vanadium monoxide molecule. J Phys Chem 89:4613–4617.

Engeser M, Schlangen M, Schröder D, Schwarz H. 2003. Alkane oxidation by VO_2^+ in the gas phase: A unique dependence of reactivity on the chain length. Organometallics 22:3933–3943.

Engeser M, Schröder D, Schwarz H. 2005. Gas-phase dehydrogenation of methanol with mononuclear vanadium-oxide cations. Chem Eur J 11: 5975–5987.

Farber M, Srivastava RD, Uy OM. 1972. Efusion mass spectrometric determination of heats of formation of gaseous molecules V_4O_{10}, V_4O_8, VO_2, and VO. J Chem Phys 56:5312–5315.

Feyel S, Schröder D, Schwarz H. 2006. Gas-phase oxidation of isomeric butenes and small alkanes by vanadium-oxide and -hydroxide cluster cations. J Phys Chem A 110:2647–2654.

Fielicke A, Rademann K. 2002. Stability and reactivity patterns of medium-sized vanadium oxide cluster cations $V_xO_y^+$ ($4 \leq x \leq 14$). Phys Chem Chem Phys 4:2621–2628.

Fielicke A, Mitrić R, Meijer G, Bonačić-Koutecký V, von Helden G. 2003. The structures of vanadium oxide cluster-ethene complexes. A combined IR multiple photon dissociation spectroscopy and DFT calculation study. J Am Chem Soc 125:15716–15717.

Fielicke A, Ratsch C, von Helden G, Meijer G. 2005. Isomer selective infrared spectroscopy of neutral metal clusters. J Chem Phys 122:091105.

Fielicke A, Rabin I, Meijer G. 2006. Far-infrared spectroscopy of small neutral silver clusters. J Phys Chem A 110:8060–8063.

Gause O. 2004. Infrarot-Photodissoziations Spektroskopie an $V_3O_7^+$ und $V_3O_8^+$ in der Gasphase mittels Argon Messenger Atomen. Diploma thesis. Freie Universität Berlin.

Gerhards M. 2004. High energy and narrow bandwidth mid IR nanosecond laser system. Opt Commun 241:493–497.

Gerhards M, Unterberg C, Gerlach A. 2002. Structure of a beta-sheet model system in the gas phase: Analysis of the C=O stretching vibrations. Phys Chem Chem Phys 4:5563–5565.

Grant ER, Schulz PA, Sudbo AS, Shen YR, Lee YT. 1978. Is multiphoton dissociation of molecules a statiscial process? Phys Rev Lett 40:115–118.

Green SME, Alex S, Fleischer NL, Millam EL, Marcy TP, Leopold DG. 2001. Negative ion photoelectron spectroscopy of the group 5 metal trimer monoxides V_3O, Nb_3O, and Ta_3O. J Chem Phys 114:2653–2668.

Harrington J, Weisshaar JC. 1992. State-to-state photoionization of VO: Propensity for large, positive changes in rotational quantum number. J Chem Phys 97:2809–2812.

Harvey JN, Diefenbach M, Schröder D, Schwarz H. 1999. Oxidation properties of the early transition-metal dioxide cations MO_2^+ (M = Ti, V, Zr, Nb) in the gas-phase. Int J Mass Spectrom 182/183:85–97.

Headrick JM, Bopp JC, Johnson MA. 2004. Predissociation spectroscopy of the argon-solvated $H_5O_2^+$ "zundel" cation in the 1000–1900 cm^{-1} region. J Chem Phys 121:11523–11526.

Janssens E, Santambrogio G, Brümmer M, Wöste L, Lievens P, Sauer J, Meijer G, Asmis KR. 2006. Isomorphous substitution in bimetallic oxide clusters. Phys Rev Lett 96:233401.

Johnson JRT, Panas I. 1999. Structure, bonding and redox properties of scandium oxide clusters, a model study. Chem Phys 248:161–179.

Justes DR, Castleman AW, Mitric R, Bonačić-Koutecký V. 2003a. $V_2O_5^+$ reaction with C_2 H_4: Theoretical considerations of experimental findings. Eur Phys J D 24:331–334.

Justes DR, Mitric R, Moore NA, Bonačić-Koutecký V, Castleman AW Jr. 2003b. Theoretical and experimental consideration of the reactions between $V_xO_y^+$ and ethylene. J Am Chem Soc 125:6289–6299.

Justes DR, Moore NA, Castleman AW Jr. 2004. Reactions of vanadium and niobium oxides with methanol. J Phys Chem B 108:3855–3862.

Kaposta C. 2005. Gas phase infrared photodissociation spectroscopy of mass selected cluster ions: Strong hydrogen bonds and vanadium oxides. Ph.D. thesis. Freie Universität Berlin.

Kasai PH. 1968. ESR of VO in argon matrix at establishment of its electronic ground state. J Chem Phys 49:4979–4984.

Keenan PC, Schroeder LW. 1952. An infrared system of bands of VO in M-type stars. Astrophys J 115:82–88.

Knight LB Jr, Babb R, Ray M, Banisaukas TJ III, Russon L, Dailey RS, Davidson ER. 1996. An electron spin resonance investigation of vanadium dioxide and VO in neon matrices with preliminary assignments for VO_3 and V_2^+: Comparison with ab initio theortical calculations. J Chem Phys 105:10237–10250.

Knippels GMH, Van Werkhoven GHC, Haselhoff EH, Faatz B, Oepts D, Van Amersfoort PW. 1995. Influence of the radial mode structure on the losses in the felix hole-coupled resonators. Nucl Instrum Meth A 358:308–310.

Koyanagi GK, Bohme DK, Kretzschmar I, Schröder D, Schwarz H. 2001. Gas-phase chemistry of bare V^+ cation with oxygen and water at room temperature: Formation and hydration of vanadium oxide cations. J Phys Chem A 105:4259–4271.

Krusin-Elbaum L, Newns DM, Zeng H, Derycke V, Sun JZ, Sandstrom R. 2004. Room-temperature ferromagnetic nanotubes controlled by electron or hole doping. Nature 431:672–676.

Kuyanov KE, Momose T, Vilesov AF. 2004. Solid hydrogen Raman shifter for the mid-infrared range (4.4–8 mu m). Appl Opt 43:6023–6029.

Lagerqvist A, Selin LE. 1957. Some infrared bands of vanadium oxide. Arkiv för Fysik 11:429–430.

Lee C, Yang W, Parr RG. 1988. Development of the Colle-Salvetti correlation-energy formula into a functional of the electron density. Phys Rev B 37:785–789.

Matsuda Y, Bernstein ER. 2005. Identification, structure, and spectroscopy of neutral vanadium oxide clusters. J Phys Chem A 109:3803–3811.

Merer AJ. 1989. Spectroscopy of the diatomic 3D transition metal oxides. Annu Rev Phys Chem 40:407–438.

Moore NA, Mitric R, Justes DR, Bonačić-Koutecký V, Castleman AW. 2006. Kinetic analysis of the reaction between $(V_2O_5)_{n=1,2}^+$ and ethylene. J Phys Chem B 110:3015–3022.

Nee M, Kaposta C, Osterwalder A, Cibrian Uhalte C, Xie T, Kaledin A, Carter S, Bowman JM, Meijer G, Neumark DM, Asmis KR. 2004. Investigating the vibrational structure of $BrHI^-$ and $BrDI^-$ with infrared predissociation and resonant multiphoton dissociation. J Chem Phys 121:7259.

Oepts D, van der Meer AFG, van Amersfoort PW. 1995. The free-electron-laser user facility felix. Infrared Phys Technol 36:297–308.

Okumura M, Yeh LI, Lee YT. 1985. The vibrational predissociation spectroscopy of hydrogen cluster ions. J Chem Phys 83:3705–3706.

Oomens J, Meijer G, von Helden G. 2001. Gas phase infrared spectroscopy of cationic indane, acenaphthene, fluorene, and fluoranthene. J Phys Chem A 105:8302–8309.

Oomens J, Tielens AGGM, Sartakov BG, von Helden G, Meijer G. 2003. Laboratory infrared spectroscopy of cationic polycyclic aromatic hydrocarbon molecules. Astrophys J 591:968–985.

Oomens J, Sartakov BG, Meijer G, von Helden G. 2006. Gas-phase infrared multiple photon dissociation spectroscopy of mass-selected molecular ions. Int J Mass Spectrom 254:1–19.

Pacchioni G, Frigoli F, Ricci D, Weil JA. 2001. Theoretical description of hole localization in a quartz Al center: The importance of exact electron exchange. Phys Rev B 63:054102.

Putter M, von Helden G, Meijer G. 1996. Mass selective infrared spectroscopy using a free electron laser. Chem Phys Lett 258:118–122.

Pykavy M, van Wüllen C. 2003. Multireference correlation calculations for the ground states of VO^{+0-} using correlation consistent basis sets. J Phys Chem A 107:5566–5572.

Pykavy M, van Wüllen C, Sauer J. 2004. Electronic ground states of the $V_2O_4^{+/0/-}$ species from multi-reference correlation and density functional studies. J Chem Phys 120:4207–4215.

Raffy J, Debuisschert T, Pocholle JP, Papuchon M. 1994. Tunable laser source with optical parametric oscillators in series. Appl Opt 33:985–987.

Reynolds MS, Butler A. 1996. Oxygen-17 NMR, electronic, and vibrational spectroscopy of transition metal peroxo complexes: Correlation with reactivity. Inorg Chem 45:2378–2383.

Robertson WH, Johnson MA. 2003. Molecular aspects of halide ion hydration: The cluster approach. Annu Rev Phys Chem 54:173–213.

Rosenbaum NH, Owrutsky JC, Tack LM, Saykally RJ. 1986. Velocity modulation laser spectroscopy of negative-ions—The infrared-spectrum of hydroxide (OH^-). J Chem Phys 84:5308–5313.

Rudnyi EB, Kaibicheva EA, Sidorov LN. 1993. Negative ions VO_2^-, VO_3^-, $V_2O_5^-$, $V_3O_8^-$ and $V_4O_{10}^-$ in the vapors of vanadium oxides. Determining enthalpies of formation from equilibrium constants. J Chem Therm 25:929–947.

Rynbrandt JD, Rabinovitch BS. 1971. Direct demonstration of nonrandomization of internal energy in reacting molecules. Rate of intramolecular energy relaxation. J Chem Phys 54:2275–2276.

Santambrogio G. 2001. IR Photodissociation and Femtosecond Negative-Neutral-Positive Spectroscopy of Vanadium Oxide Clusters and Clusters Ions. Diploma thesis. Universita' Degli Studi di Milano.

Santambrogio G, Brümmer M, Wöste L, Döbler J, Sierka M, Sauer J, Meijer G, Asmis KR. 2007. Gas Phase Infrared Spectroscopy of Mass-Selected Vanadium Oxide Cluster Anions. Submitted to J Chem Phys.

Sauer J, Döbler J. 2004. Structure and reactivity of V_2O_5: Bulk solid, nanosized clusters, species supported on silica and alumina, cluster cations and anions. Dalton Trans 19:3116–3121.

Schröder D, Loos J, Engeser M, Schwarz H, Jankowiak H-C, Berger R, Thissen R, Dutuit O, Döbler J, Sauer J. 2004. Ion chemistry of $OV(OCH_3)_3$ in the gas phase: Molecular cations and anions and their primary fragmentations. Inorg Chem 43:1976–1985.

Schröder D, Engeser M, Schwarz H, Rosenthal ECE, Döbler J, Sauer J. 2006. Degradation of ionized $OV(OCH_3)_3$ in the gas phase. from the neutral compound all the way down to the quasi-terminal fragments VO^+ and VOH^+. Inorg Chem 45:6235–6245.

Sherrill CD, Lee MS, Head-Gordon M. 1999. On the performance of density functional theory for symmetry-breaking problems. Chem Phys Lett 302:425–430.

Siegel RW, Hu E, Roco MC. 1999. Nanostructure Science and Technology: R&D Status and Trends in Nanoparticles, Nanostructured Materials, and Nanodevices. In: Nanostructure science and technology: A worldwide study. Loyola College, Maryland.

Sodupe M, Bertran J, Rodriguez-Santiago L, Baerends EJ. 1999. Ground state of the $(H_2O)_2^+$ radical cation: DFT versus post-Hartree-Fock methods. J Phys Chem A 103:166–170.

Solans-Monfort X, Branchadell V, Sodupe M, Sierka M, Sauer J. 2004. Electron hole formation in acidic zeolite catalysts. J Chem Phys 121:6034–6041.

Sudbo AS, Schulz PA, Shen YR, Lee YT. 1986. Molecular-beam studies of laser-induced multiphoton dissociation. In: Cantrell CD, editor. Multiple-photon excitation and dissociation of polyatomic molecules. Berlin: Springer-Verlag. pp 95–122.

Tepper B, Richter B, Dupuis AC, Kuhlenbeck H, Hucho C, Schilbe P, bin Yarmo MA, Freund H-J. 2002. Adsorption of molecular and atomic hydrogen on vacuum-cleaved $V_2O_5(001)$. Surf Sci 496:64–72.

von Helden G, Holleman I, Knippels GMH, van der Meer AFG, Meijer G. 1997. Infrared resonance enhanced multiphoton ionization of fullerenes. Phys Rev Lett 79:5234–5237.

von Helden G, Kirilyuk A, van Heijnsbergen D, Sartakov B, Duncan MA, Meijer G. 2000. Infrared spectroscopy of gas-phase zirconium oxide clusters. Chem Phys 262:31–39.

von Helden G, van Heijnsbergen D, Meijer G. 2003. Resonant ionization using IR light: A new tool to study the spectroscopy and dynamics of gas-phase molecules and clusters. J Phys Chem A 107:1671–1688.

Vyboishchikov SF, Sauer J. 2000. Gas-phase vanadium oxide anions: Structure and detachment energies from density funtional calculations. J Phys Chem A 104:10913–10922.

Vyboishchikov SF, Sauer J. 2001. $(V_2O_5)_n$ gas-phase clusters (n-1-12) compared to V_2O_5 Crystal: DFT calculations. J Phys Chem A 105: 8588–8598.

Walker NR, Walters RS, Tsai M-K, Jordan KD, Duncan MA. 2005. Infrared photodissociation spectroscopy of $Mg^+(H_2O)Ar_n$ complexes: Isomers in progressive microsolvation. J Phys Chem A 109:7057–7067.

Weckhuysen BM, Keller DE. 2003. Chemistry, spectroscopy and the role of supported vandium oxides in heterogeneous catalysis. Catal Today 78:25–46.

Whittingham MS. 2004. Lithium batteries and cathode materials. Chem Rev 104:4271–4301.

Wu H, Wang L-S. 1998. A photoelectron spectrsocopic study of monovanadium oxide anions (VO_x^-, x = 1–4). J Chem Phys 108: 5310–5318.

Zemski KA, Justes DR, Castleman AW Jr. 2001. Reactions of group V transition metal oxide cluster ions with ethane and ethylene. J Phys Chem A 105:10237–10245.

Zemski KA, Justes DR, Castleman AW. 2002. Studies of metal oxide clusters: Elucidating reactive sites responsible for the activity of transition metal oxide catalysts. J Phys Chem B 106:6136–6148.

Zhai HJ, Wang L-S. 2002. Electronic structure and chemical bonding of divanadium oxide clusters (V_2O_x, x = 3–7) from anion photoelectron spectroscopy. J Chem Phys 117:7882–7888.

Knut R. Asmis received his Dr. rer. nat. in Physical Chemistry from the Université de Fribourg, Switzerland in 1996. After his Postdoctoral fellowship in the group of Daniel Neumark at the University of California, Berkeley, he joined the group of Ludger Wöste in 1999 and earned his Habilitation in Experimental Physics from the Freie Universität Berlin in 2006. Since 2005 he is a Research Group Leader at the Fritz-Haber-Institut of the Max-Planck-Gesellschaft in Berlin, where he continues to develop new techniques to study the vibrational spectroscopy of gas phase ions, with emphasis on hydrogen bonding, ion and electron solvation as well as the structure, dynamics and reactivity of transition metal oxide clusters.

Joachim Sauer received the Dr. rer. nat. degree in Chemistry from Humboldt University in Berlin in 1974. He joined the Central Institute of Physical Chemistry of the (former) Academy of Sciences in (East-)Berlin in 1977, receiving the Dr. sc. nat. degree from the Academy in 1985. Since 1993 he is Professor of Physical and Theoretical Chemistry at the Humboldt University in Berlin, and in 2006 he became an external member of the Fritz Haber Institute in Berlin (Max Planck Society). He is member of the ''Berlin-Brandenburgische Akademie der Wissenschaften.'' His research has explored the application of quantum chemical methods in chemistry, with emphasis on surface science, particularly adsorption and catalysis. He has published more than 200 research papers, notably in the area of modeling the structure and reactivity of solid catalysts including zeolites and transition metal oxides. He is chairman of the Collaborative Research Center of the German Science Foundation ''Aggregates of transition metal oxides–Structure, dynamics, reactivity.''